CHARLES UNIVERSITY PRAGUE

faculty of mathematics and physics

Structure, Thermal and Physical Properties of Liquid Crystalline Polymers

Alexander Jigounov

Prague 2007

Acknowledgements

First of all, I would like to thank my supervisor Prof. Ing. Michal Ilavský, DrSc. for encouraging me and offering me opportunity to start my Ph.D. study.

I would like to thank to Doc. RNDr. Jan Nedbal, CSc. for very valuable contribution into discussions and for the time he spent helping me with evaluation of dielectric results.

Many thanks belong also to Zdeňka Sedláková, PhD from the Institute of Macromolecular Chemistry for sample preparation.

I would like to thank to Prof. Polycarpos Pissis from National Technical University of Athens for my pleasure staying in Greece and possibility to make dielectric measurements in his laboratory. Many thanks to Roula Kripotou for advising in dielectric measurements and data analyze.

I'm also very grateful to the RNDr. Helena Valentova, Ph.D. for her help in the beginning of my mechanical measurements, for guiding me and tons of advising. Also she was the person who inspired me to learn Czech language and I'm very thankful for this too.

I would like to thank many people including my colleagues and people working at other groups, for their lectures, valuable discussions and detailed explanations at many fields.

And at last, but not the least, I would like to thank my family and my friends, Alenichev Igor, Konstantyn Tuharyn, Volozhina Natalia, Grinevich Andrey and many others.

Financial support of the Grant Agency the Academy of Sciences of the Czech Republic (grant No. IAA4112401) and of the Ministry of Education, Youth and Sports of the Czech Republic (grant MSM 0021620835) is gratefully acknowledged.

Contents

1. Introduction

Polymeric materials and their physical properties have been widely studied for a long time and during this period they have found practical applications in many industrial areas. However, they were used also in variety special fields, including photonic, ferroelectric and antiferroelectric applications. Introduction of rigid mesogenic groups into the polymer chain (backbone (MC) or side-chain (SC)) usually leads to liquid-crystalline polymers (LCPs), which show an intermediate state of aggregation between the crystalline and amorphous structures [1-4]. The meaning of the phrase "liquid crystal" is coming from confrontation of solid state crystal structure with liquids. Whilst solid crystalline lattice is characterized with 3-dimensional periodical order of atoms or molecules, in liquids no long-range order exists. On the other side, there exists a series of organic low-molecular materials, called liquid crystals, which exhibit a phase of a matter that are characterized by properties between those of a conventional liquids, and those of a solid crystals. For instance, a liquid crystal (LC) may flow like a liquid, but the molecules in the liquid are arranged and/or oriented in a crystal-like way. The driving forces for formation of molecular order in LCPs are the shape of mesogens, flexibility of polymer chain, and miscibility of initial reactants. Such materials, with more ordered smectic or less ordered nematic structure, usually show an improved mechanical and other physical properties. There are two basic types of LCPs – lyotropic and thermotropic ones. While in the first group the LC materials exhibit changes of the structure with concentration of solvent (LC properties) the change of the structure of the second group is due to the change of temperature.

Interesting LC-systems are formed if mesogenic groups are combined with flexible spacers, such as $(CH_2)_n$, because both LC and isotropic states are present in such polymers. Side-chain LC polymers (SCLCPs) with flexible backbone and mesogenic groups in side-chains have also been an active area of research. Such systems, especially with azobenzene moieties in side-chains (azopolymers), have been extensively studied in recent years [5-8]. Azopolymers form a class of photochromic materials in which usually birefringence and optical dichroism, based on cis/trans photoisomerisation of azochromophores, can be initiated by polarized light since the transition dipole moment of azobenzene groups is oriented along the molecular axis of elongated trans-isomer; dichroism and birefringence can be erased by subsequent irradiation with non-polarized

light [9-11,16]. Stability of dichroism and birefringence depend on molecular motions in polymer.

Most of thermal and physical investigations were made on SCLCPs based on polyacrylates and polysiloxanes [3, 4, 11]. In our work we have used as the flexible backbone polybutadiene diol (PBD). In this case reactive double bonds are available in each 1,4 or 1,2 monomeric unit for grafting of mesogenic LC thiol using an addition reaction of SH group onto double bonds of PBD. In such a way the side-chains of various LC structures (containing flexible spacers and mesogens of various types) can be grafted onto the polybutadiene backbone and side-chains LC- polybutadienes (SCLCPBDs) can be synthesized.

Dielectric relaxation spectroscopy in broad frequency and temperature regions is an effective tool for characterization of molecular motions in polymer systems [12-16] as various relaxation mechanisms can be expressed in terms of relaxation times and their temperature dependences, magnitude and shape of dielectric response. For LCPs it was found that the dependences of dielectric functions on frequency and temperature are sensitive to the ordered mesomorphic state due to more or less aligned parts of macromolecular chains. Also the dynamic mechanical spectroscopy was often used for investigation of LC polymers [13, 14]; it was found that the dependences of mechanical functions on frequency and temperature are sensitive to the ordered state of macromolecules; mechanical behavior similarly to the dielectric ones in the LC-state reflects the coupled response of ordered mesogenic groups to an applied force. The structural transitions detected by differential scanning calorimetry (DSC), polarizing microscopy and wide-angle X-ray scattering are also observed in dielectric and mechanical measurements [15].

This thesis is concerned with an experimental investigation of the relations between structure and thermal, dynamic mechanical and dielectric behavior of side-chains liquid-crystalline polybutadiene-diol (SCLCPBDs) in a broad frequency and temperature regions. Two types of thiols with various structure of mesogenic group (cyanobiphenyl or azobenzene) were synthesized and used for preparation of comb-like polybutadiene-diols (PBD). In Part 2 the description of different structural modifications of LCPs is given. The experimental results obtained on various LCPs in literature are discussed in Part 3. The aims of thesis are given in Part 4. Materials and methods of measurements used in thesis are described in Part 5. Main obtained results and their discussion is given in Part 6. Finally, conclusions, which follow from obtained results, are presented in Part 7.

2. Theoretical Review

2.1 Structures of liquid-crystalline polymers

2.1.1 Thermotropic liquid crystal polymers

Thermotropic liquid-crystalline polymers are interesting materials due to their technological importance; they are relatively good of manufacturing products with outstanding mechanical properties. Easy molecular orientation is the result of the liquid-crystalline structure of the melt in a temperature region between the semi-crystalline state and the isotropic-melt state, resulting in relative low viscosity. The liquid-crystalline state is the consequence of the rigidity of the molecules, which are spontaneously ordered along a mean direction, called the director *n*. There are many different types of LC phases, which can differ in their resulting optical properties (such as birefringence). When viewed under a microscope, using a polarized light source, different liquid crystal phases will appear to have a distinct texture. Each "patch" in the texture corresponds to a domain where the LC molecules are oriented in a different direction. Within a domain, however, the molecules are quite well ordered.

Thermotropic liquid-crystalline polymers belong to a relatively new class of liquid-crystalline compounds. Indeed, if lyotropic polymeric liquid crystals (such as, for instance, solutions of synthetic polypeptides) have been well-known and are under investigation already for quite a long time, the first attempts to synthesize thermotropic polymeric liquid crystals date only to the beginning of the 70th of the last century. It is in this period, based on extensive interest in practical utilization of low-molecular liquid crystals, publications revealing various approaches towards synthesis of thermotropic LC polymers systems begin to appear and mesomorphic polymers become the object of intensive attention of scientists, working in the field of polymer science. The study of this type of polymers is of interest in its own right, which is inspired by the need to clarify the nature and specific features of LC state of macromolecular compounds [17-20].

On the other hand, the interest towards this field is caused by the possibility to create such polymeric systems which combine the unique properties of low-molecular liquid crystals and high molecular polymer compounds, making it feasible to produce films, fibers and coatings with extraordinary features. It is known that the utilization of low-molecular thermotropic liquid crystals requires special hermetic protective shells (electrooptical cells, microcapsules etc.), which maintain their shape and protect LC compounds from external influences. In the case of thermotropic LC polymers there is no

need for such sandwich-like constructions, because the properties of low-molecular liquid crystals and of polymer chains are combined in a single individual material. This reveals essentially new perspectives for their application.

At present at least three types of thermotropic LC polymers may be identified - these are:

1) the melts of some linear crystallizable polymers
2) polymers with mesogenic groups incorporated in the backbone
3) polymers with mesogenic side groups

Thermotropic phases are ordered phases those that occur in a certain temperature range. If the temperature is raised, thermal motion will destroy the cooperative ordering of the LC phase, pushing the material into a conventional isotropic phase. At too low temperature, most LC materials will form conventional (though anisotropic) crystals. Many thermotropic LCs exhibit a variety of phases as temperature is changed. For instance, a particular mesogen may exhibit various smectic and nematic (and finally isotropic) phases as temperature is increased.

The various LC phases (called mesophases) can be characterized by the type of ordering that is present [19-21]. One can distinguish positional order (molecules are arranged in any sort of ordered lattice) and orientational order (molecules are mostly pointing in the same direction), and moreover order can be either short-range (only between molecules close to each other) or long-range (extending to larger, sometimes macroscopic, dimensions). Most thermotropic LCs will have an isotropic phase at high temperatures. That is, heating will eventually drive them into a conventional liquid phase, characterized by random and isotropic molecular ordering (no long-range order), and fluid-like flow behavior. Under other conditions (for instance at lowering temperature), a LC might inhabit one or more phases with significant anisotropic orientational structure and long-range orientational order while still having an ability to flow.

The ordering of liquid crystalline phases is extensive on the molecular scale. This order extends up to the entire domain size, which may be on the order of micrometers, but usually does not extend to the macroscopic scale as often occurs in classical crystalline solids. However, some techniques (such as the use of boundaries or an applied electric field) can be used to enforce a single ordered domain in a macroscopic liquid crystal sample. The ordering in a LC might extend along only one dimension, with the material being essentially disordered in the other two directions.

2.1.2 Nematic phase in polymers

One of the most common LC phase in polymeric materials is the nematic one [19], where the molecules have no positional order, but they do have long-range orientational order. Thus, the molecules flow and their centre of mass positions are randomly distributed as in a liquid, but they all point in the same direction (within each domain). Most nematics are uniaxial - they have one axis that is longer and preferred, with the other two being equivalent (can be approximated as cylinders). Some liquid crystals are biaxial nematics, meaning that in addition to orienting their long axis, they also orient along a secondary axis.

The molecules in thermotropic LC are typically rod-shaped organic moieties about 2.5 nanometers in length and their ordering is a function of temperature. The nematic phase, for example, is characterized by the orientational order of the constituent molecules. The molecular orientation (and hence their optical properties) can be controlled with applied electric fields. Nematics are the most commonly used phases in liquid crystal displays (LCDs), with many such devices using the twisted nematic geometry.

2.1.3 Smectic phase

The more ordered liquid crystals form the so-called “smectic” mesophases which are found at lower temperatures in comparison to the nematic one. In smectics, the molecules are arranged in well defined layers so that they do have long range positional order in one dimension, perpendicular to the layer plane (layer normal). The smectics can occur in a variety of forms because within the layers there may be different arrangements and degrees of order accounting for the various classifications [19] (A-, C- phase etc.). In the Smectic A phase, the molecules are oriented along the layer normal, while in the Smectic C phase they are tilted away from the layer normal.. There is a very large number of different smectic phases, all characterized by different types and degrees of positional and orientation order 19-21].

2.1.4 Side-chain liquid crystal polymers

Traditionally two major classes of LCPs have been identified: so-called main-chain and side-chain types. The concept of the LCPs is fairly self-explanatory from its name [21]:

- Main-chain LCPs - the mesogenic (rigid) units are part of polymer main chain. Thus usually rodlike polymers are formed.
- Side-chain LCPs - the mesogenic units are attached to a (flexible) polymer backbone usually trough flexible spacer (their properties are reviewed by Finkelmann, Rehage and McArdle) [20-21].

Fig. 1 provides schematically the structure of both, main- and side-chain LCPs. The synthesis and properties of these materials have been extensively investigated [18, 22-26].

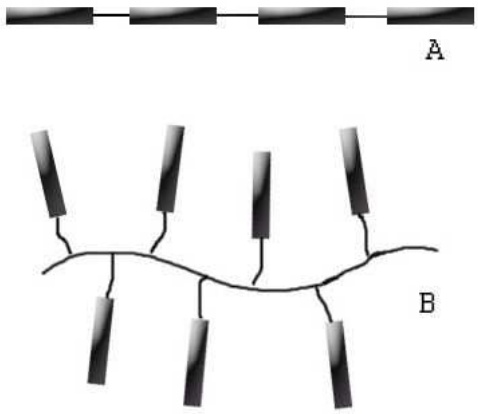

Fig 1. *Schematic representation of a main-chain LCP (A) and a side-chain LCP (B)*

2.2 Mechanical spectroscopy of polymers

Mechanical spectroscopy is an experimental technique of material characterization in which deformation and flow behavior of materials is analyzed by means of static or dynamic mechanical methods [27]. Experimental data are usually obtained from the material response to periodical variation of external mechanical stress or strain field. Material responds to the applied external stress or strain by dissipating the input energy in a viscous flow (non reversible response) and by storing the energy elastically (reversible response), or through a combination of both of these two extremes. The mechanical behavior is often a main criterion for a possibility of practical application

of these materials even if other physical properties could be obtained and used more effectively (optical, electric, etc.). The mechanical spectroscopy is also widely used experimental technique for analysis of the structure on molecular level and molecular motion in complex polymeric systems.

Despite the structural and related mechanical complexity of polymeric materials, the phenomenological description of the mechanical behavior of the systems is based on rather simple models - combination of elastic springs and damping piston [12, 27]. The two simplest limits – the elastic behavior of ideal solid (spring) and the viscous behavior of Newtonian liquid (piston) – are characterized by the well-known linear relationships between shear stress σ (force per sample area) and the shear strain γ; the relations are given either by Hook's (eq. (1)) or Newton's law (eq. (2)), respectively:

$$\sigma = G \cdot \gamma \qquad (1)$$

$$\sigma = \eta \frac{d\gamma}{dt} \qquad (2)$$

where G is the shear modulus and η is the shear viscosity.

Polymers are usually considered as viscoelastic materials in which mechanical properties strongly depend on time or frequency and on temperature. The simplest viscoelastic behavior can be represented by a Maxwell model, which is characterized by the serial connection of spring and piston. For this model the time dependence of the shear stress $\sigma(t)$ is described by equation $\sigma(t) = \sigma_0 \, \mathrm{e}^{-t/\tau}$, where the relaxation time $\tau = \eta/G$ denote the time when the stress σ decreases to the value of σ_0/e. The Maxwell model describes the viscoelastic dynamic transition between the elastic and viscose regimes which is located between times shorter (higher frequencies) and longer (lower frequencies) then the relaxation time. The mechanical behavior of real polymers is usually characterized by many relaxation times. Each relaxation time usually means a switching on and off of particular type of molecular motion in the system and separates dynamically different states of the material.

The mechanical behavior of side-chain LCPs has been studied for some thermotropic systems. One of the main difficulties of the experiments with thermotropes consists in necessity to measure at high temperatures. At these temperatures physical and chemical changes in LCPs may take place, resulting in a sensitivity of the sample to the thermal history and to a time dependences of the measuring properties [28]. The

mechanical behavior of SCLCPs was reviewed with an emphasis on experimental results by Porter and Johnson in 1967. They noted an ease of orientation of liquid crystals by electromagnetic fields and by mechanical stress, and found that this orientation is affected by the viscosity value. Orientation induced a magnetic field causes a four-fold change of viscosity in the nematic state, but has no effect in the isotropic state of sample. Also, the viscosity of the nematic fluid is lower than that of the isotropic fluid, even though the temperature is lower.

The three-region viscosity (flow) curve (Fig. 2) proposed by Onogi and Asada [29] is used as a framework for the discussion of the liquid crystal polymer rheology:

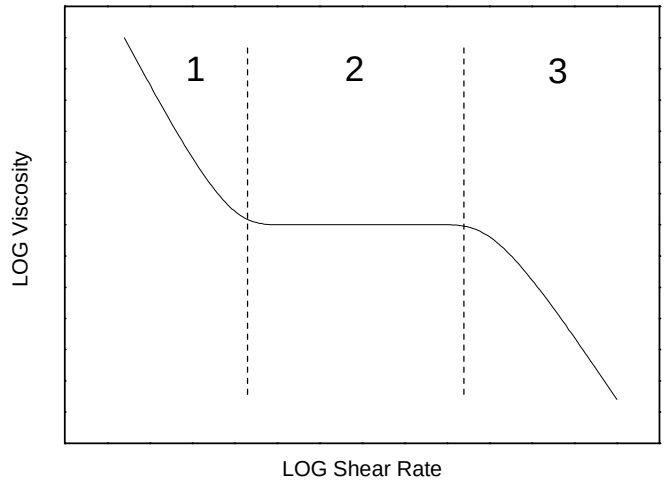

Fig. 2. *Three regions of flow behavior (from Onogi and Asada)*

A similar flow curve had been proposed earlier, with a different molecular interpretation, by Pochan and co-workers for cholesteric mesophases; the explanation was based on rheo-optical (combination of mechanical and deformational birefringence measurements) studies.

On the basis of the published evidence, one cannot say very much about the shear thinning of Region 3 [29]. The data are simply too inconsistent. The phenomena associated with Region 1 are even more complex. The first challenge now is for experimentalists to define the conditions of their experiments sufficiently and to learn for each studied system what the variables of sample history are and how they affect the flow behavior. The second challenge then will be to control and specify the morphology or texture of measured materials in order to study how the texture is affected by deformation.

2.2.1 Principles of mechanical analysis

Force (or stress – force per unit crossection) and deformation (change of the sample shape) are the two physical quantities which accompany any mechanical measurement of the material. The mechanical experiment consists in determination of the relations between stress and deformation (strain). Depending on the way in which the forces are applied to the material, various kinds of deformations can be distinguished and various components of the more general relations between strains and stresses can be determined. As examples, tension, simple shear and compression are illustrated in Fig. 3:

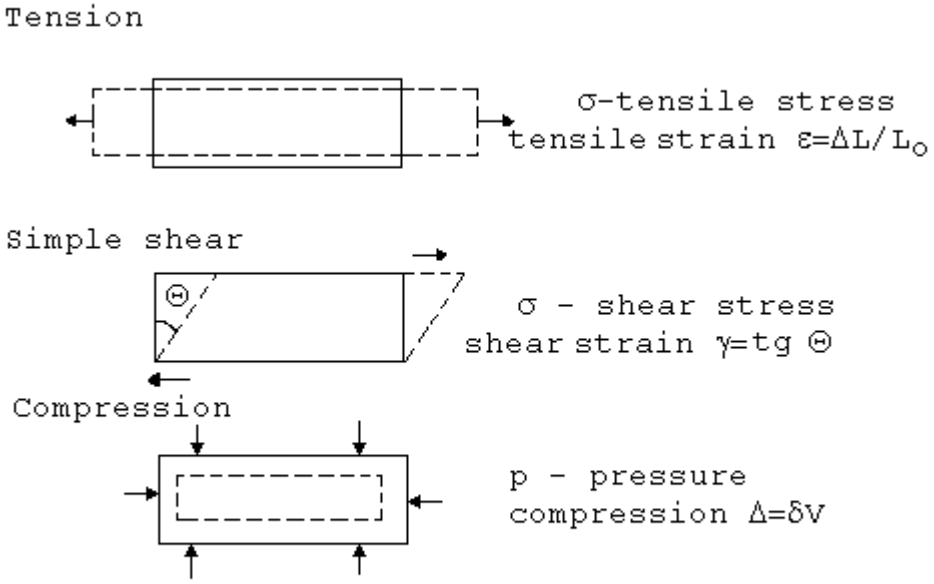

Fig. 3. *Examples of different types of deformations*

For materials, the three types of the deformations allow one to determine the Young's modulus in extension ($E = \sigma/\varepsilon$), the shear modulus ($G = \sigma/\gamma$), and the compression modulus ($K = p/\Delta$) as the ratios of corresponding stresses and deformations. The measurements of mechanical properties can generally be considered as an input - output system in which the input signal, in the form of time (or frequency) dependent force or deformation, is applied to a sample and the output signal is resulting deformation or force monitored in dependence on time (or frequency); environmental conditions, such as temperature, humidity etc. can also be taken into account. Usually in dynamic mechanical experiments, a sinusoidal strain is applied to a material and the resulting stress is recorded. The stress signal is then separated into two components: an elastic (real) component (which is in phase with the applied strain) and a viscous (imaginary)

component (which is 90^o out of phase with the strain). In this way, information's on both the elastic and viscous component are determined.

2.2.2 The dependence of mechanical behavior on frequency or time

To define dynamic mechanical properties of polymeric materials, the complex mechanical shear modulus is introduced. In polymers it is a function of angular frequency ω (or frequency $f = \omega/2\pi$), temperature T and some other external parameters [30]: Usually harmonically oscillations of deformation $\gamma^*(t)$ are applied on material in the form:

$$\gamma^*(t) = \gamma_0 \exp(i\omega t) \qquad (3)$$

where γ_0 corresponds to the amplitude deformation and i is imaginary unit. In this case linear viscoelasticity theory can be applied and the stress $\sigma^*(t)$ in sample follows the same frequency as deformation, but with a phase shift δ:

$$\sigma^*(t) = \sigma_0 \exp\ i(\omega t + \delta) \qquad (4)$$

where σ_0 is the stress amplitude. The complex shear modulus G^* is than given by the equation:

$$G^* = \frac{\sigma^*}{\gamma^*} = \frac{\sigma_0}{\gamma_0}\exp i\delta = \frac{\sigma_0}{\gamma_0}(\cos(\delta) + i\sin(\delta)) = G' + iG'' \qquad (5)$$

The real part of the modulus G' is called elastic (storage) modulus (it is in phase with deformation) and imaginary (loss) part G'' is called viscous modulus (is shifted 90 ^{o} from deformation); also the loss tangent tan $\delta = G''/G'$ is often used in mechanical measurements. Elastic modulus is associated with an elastic energy stored in the sample; the volume density of elastic energy could be expressed by:

$$w_E = \int_0^{\gamma_0} G'\gamma d\gamma \qquad (6)$$

Viscous modulus corresponds to the energy losses with deformation; volume density of the dissipative energy could be expressed by:

$$w_D = \int_0^{\gamma_0} \frac{G''}{\omega} \dot{\gamma} d\gamma \qquad (7)$$

In the Fig. 4 one can see the dependence of elastic modulus *G'* on frequency at constant temperature. This figure is the typical for mechanical behavior of amorphous linear polymers. It is possible to distinguish on the curve four regions:

1. Glassy state region (at the highest frequencies *f*)
2. Main-glass transition region (intermediate *f*)
3. Rubbery plateau region (low *f*)
4. Flow region (the lowest *f*)

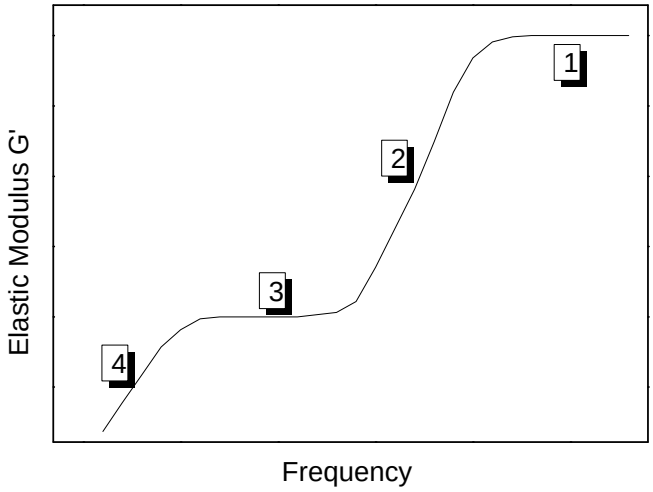

Fig. 4. *Dependence of real (storage) modulus G' on frequency at constant temperature*

At the highest frequencies (region 1) the polymer is in so-called glassy state. This region is characterized by the very high values of modulus *G'*. For many polymeric materials in this region one can observe small changes in modulus values, which are associated with so-called secondary relaxations (movement of side-chains or small part of main-chain groups). Deformation in this region leads to such processes as conformational changes or rotations of the short parts of polymer chain. The frequencies of these

movements strongly depend on chemical structure and geometry of the monomer units. The movement of the whole main-chain is freezed in this region.

The most pronounced changes in *G'* modulus (several orders of magnitude) with the frequency (or temperature) is observed in region 2. This is the main transition region from the glassy-state to the rubber-like state (glass transition region). In this region modulus decreases for 3-4 logarithmic decades and the main-chain motion is subsequently released.

In the rubbery plateau region (region 3) cooperative motion of whole network chains are already realized. Usually inter-chain interactions (permanent entanglements) prevent the movement of whole polymer molecules and system behaves as physically crosslinked network. Finally at the lowest frequencies (flow region 4) polymer molecules can freely flow and macro-Brownian motion is allowed.

2.2.3 Time-Temperature superposition

When amorphous polymer above the glass transition temperature T_g is deformed, its chains try to obtain the most probable configurations which correspond to deformed state. The rate of the configurational changes depends on local viscosity, which decreases with increasing temperature. From this it follows that the interrelations between time- and temperature- dependences of mechanical behavior exist; these mutual relations were expressed in time-temperature superposition principle [27]. This principle is very useful and was confirmed by many experimental studies; it was also included in the molecular theories of viscoelastic behavior.

The most important assumption of the superposition principle is that the influence of the temperature changes affects all relaxation times by the same value. This mean that the shape of mechanical functions on time (or frequency) with temperature does not change; the functions are only shifted on time (frequency) scale. Temperature shift factor a_T is then defined as:

$$a_{T_0} = \frac{\tau_T}{\tau_{T_0}} \qquad (8)$$

where τ_T is relaxation time at temperature T and τ_{T_0} is relaxation time at chosen temperature T_0. Moreover it is supposed, that all contributions to the modulus are proportional to absolute temperature and density in accord with well-known kinetic

theory of rubber elasticity [27]. From above it follows, that the reduced curve of modulus $G_p(t)$ (which characterizes mechanical behavior at chosen temperature T_0 in a very broad frequency scale)) can be obtained from the short-term mechanical measurements of moduli $G(t)$ at different temperatures T:

$$\log G_p(t) = \log \frac{G(t)T\rho}{T_0\rho_0} \tag{9}$$

where ρ is the density of polymer at temperature T and ρ_0 is the density at temperature T_0. It was experimentally shown that the dependence of the shift factor on temperature can be described by the Williams-Landel-Ferry (WLF) equation:

$$\log a_{T_S}(T) = \frac{-8.86(T - T_S)}{101.6 + T - T_S} \tag{10}$$

where T_s is the reference temperature. It was found that for the most polymeric systems $T_S = T_g + 50\ ^oC$ (T_g is the glass transition temperature) and that the equation well describes experimental temperature dependence of the shift factor in the range: $T_S - 50\ ^oC < T < T_S + 50\ ^oC$. Further measurements have shown that the constants in equation (10) slightly depend on detailed structure of polymer and that the temperature dependence of the shift factor is better described by the equation:

$$\log a_{T_0}(T) = -\frac{C_1^0 (T - T_0)}{C_2^0 + T - T_0} \tag{11}$$

Where C_1^0 and C_2^0 are the constants for particular polymer and depend on the chosen temperature T_0. These constants were later interpreted in polymer free volume parameters. Finally, we can conclude that superposition principle is based on 3 assumptions:

1. proportionality of contribution to the modulus - ρRT
2. every relaxation time is proportional to the value of the one friction coefficient (shape of mechanical functions do not change with temperature)
3. structure of polymer does not change with the temperature.

Summarizing, one could say that the use of the superposition method allows to obtain the superimposed (master) curves of mechanical functions in very broad time (frequency)

interval by shifting of the curves measured in short time (frequency) region at various temperatures.

2.2.4 Free volume theory of viscoelasticity

In each material one can find some free space between polymer molecules. In general, in material it is possible to distinguish between the total volume and the occupied volume. The difference between these two volumes is considered to be a free volume [27]. The amount of the free volume changes with temperature. This amount can be estimated from X-ray scattering and positron annihilation experiments. Normally the volume of a single hole it is about 0.02-0.07nm^3.

Most of the theoretical models operate with the fractional free volume, *f*, which is the ratio of the free volume to the total volume. The main assumption of the free volume theory is that below the glass transition temperature T_g the free volume does not change [27]. In that case the equation for temperature dependence of the fractional free volume is:

$$f = f_g + \alpha_f (T - T_g) \qquad (12)$$

where f_g is fractional free volume at T_g and α_f is coefficient of the temperature free volume expansion. Using Doolittle equation [27] for the dependence of viscosity on the free volume - $\eta = A\exp(\frac{B}{f})$ and using equation (12) it is possible to obtain the WLF equation (11) for the shift factor (for $T_0 = T_g$) in the form:

$$\log a_{T_g}(T) = -\frac{(B/2.3 f_g)(T - T_g)}{f_g/\alpha_f + T - T_g} \qquad (13)$$

in equation (13) *B* is the constant (usually equal to 1). Usually $\alpha_f = \alpha_l - \alpha_g$, where α_g – is the coefficient of the temperature volume expansion below T_g and α_1 – is the coefficient of temperature volume expansion above T_g. It was shown that this equation predicts also the effect of the pressure, solvent concentration and the molecular weight of linear polymers. Comparison of equations (11) and (13) gives $C_1^g = B/2.3 f_g$ and $C_2^g = f_g/\alpha_f$.

It was experimentally shown that f_g is, in the first approximation, universal constant for the most amorphous polymers and its value is $f_g = 0.025 \pm 0.003$. The value of α_f for the polymeric systems changes in the range of 1.9 to $9.7 \cdot 10^{-4}$ K^{-1}. From this it follows that the glass transition occurs when the free volume reaches the critical value (free volume conception of glass transition).

Temperature T_g usually depends on heating/cooling rate as it was shown in many experimental studies (Fig. 5). On cooling of a polymer sample at a constant rate one can find that the specific volume (or specific heat) changes (decreases) linearly, however below a certain temperature the slope of the curve changes. This point where the discontinuous change occurs can be considered as a glass transition temperature (T_g). However if instead of further cooling one can let sample to equilibrate at a constant temperature below T_g the specific volume will change slowly to such extent that follows the original (prior to T_g) slope. This process of equilibration is usually called physical aging.

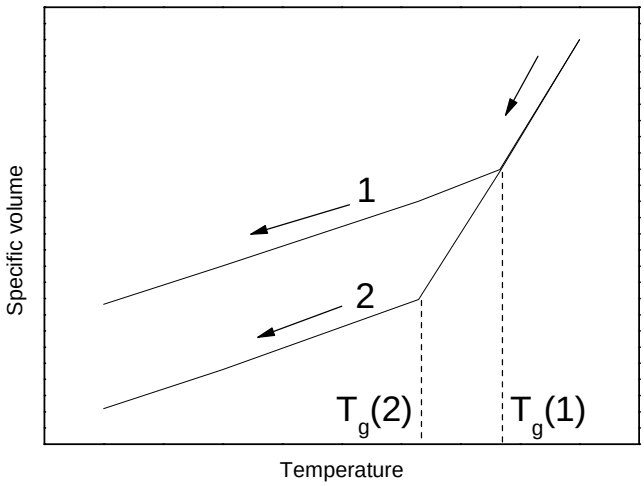

Fig. 5. *Schematic curves showing the cooling rate dependence of the specific volume of glass transition (cooling rate 1 is higher than cooling rate 2)*

The temperature dependences of the specific volume imply that the measured T_g values actually depend on the experimental conditions, such as the rate of cooling/heating (Fig. 5). The longer equilibration times before the temperature increase will result in lower value of the glass transition temperature. This evidently shows the kinetic nature of the glass transition. Since the measured specific volume depends on the temperature and rate of cooling below T_g one can take into account the time of volume recovery. The rate of recovery depends on the magnitude, sign of deviation from the reference equilibrium

state and on the fact how long the measured sample was allowed to remain at the preceding temperature (memory effects).

2.3 Dielectric spectroscopy

2.3.1 Dipole moment

The dielectric spectroscopy is based on the interaction of external electric field with matter, it means it is concerned with the microscopic mechanism of dielectric polarization. Conceptual definition of dielectric materials consists in the development of the band theory of solids [31] where the gap between the conduction and valence band is greater than 1 eV and the number of thermally generated free charges is negligible. The electric moment p of a configuration of N discrete charges q_i relative to the fixed origin is defined by equation

$$p = \sum_{i=1}^{N} q_i \cdot r_i \quad . \tag{14}$$

where the vector r_i indicates the position of point charge q_i relatively to the fixed origin. In the simplest case of two point charges $+q$ and $-q$ the electric (dipole) moment p is described by equation:

$$p = qr \tag{15}$$

where the vector r is pointing from the negative to the positive charge.

The polarization of matter in external electric field can be developed in the two most important concepts – the induced and orientation polarization. The first mechanism of polarization is active in all dielectric materials when brought into an external electric field. The second one exists only in so called polar dielectrics where the centers of positive and negative charges of a molecule do not coincide due to the non-symmetric structure of molecule even without external electric field; i.e. the molecule possesses a permanent dipole moment. The dimension of the dipole moment in SI units is [p] = C.m. The values of molecular dipole moments are still from historical reasons expressed in Debye (D) units (e.s.u.) instead of SI ones; the dipole moments of most non-symmetrical

molecules lie between 0.5 and 5 D. One Debye is: 1D = (1/3).10^{-29} C.m.

Induced dipole moment m_p is formed after application of external electric field E_l when the charge separation takes place between the outer electronic cloud and the nucleus (the atomic cores) in molecule. In this case the dipole moment m_p is proportional to the intensity E_l of the electric field according to the relation

$$m_p = AE_l \qquad (16)$$

where A is the polarizability of the molecule; the dimension of polarizability is the same as the dimension of the volume ([A] ~ m^3). This induced dipole moment adds vectorially to any permanent (orientational) dipole moment μ that a molecule may possess. Therefore the total dipole moment of polar molecule is

$$m = \mu + m_p = \mu + AE_l \qquad (17)$$

Dipole moment of non-polar molecules is determined only by the second part of equation (17), because for non-polar molecule $\mu = 0$.

The polarizability A in isotropic materials is supposed to be a constant that does not depend on external conditions (pressure and temperature) and on field intensity (if the field is rather small); in this case we have linear dielectrics. The orientation polarization was at first described by Debye [32]. He supposed that polar molecules are freely floating in a non-polar fluid and only the thermal motion has the randomizing influence on dipoles so that the mean dipole moment ‹μ› of all dipoles in a matter is equal to zero. While the dipoles oriented in the direction of external electric field E have lesser potential energy then those oriented in the opposite direction the mean dipole moment of polar matter will be under field effect (in a statistical equilibrium) non-zero. The calculation gives in the first approximation ($\mu^2 E << kT$) for the mean dipole moment ‹μ›

$$\langle \mu \rangle^2 = \frac{\mu^2}{3kT} E \qquad (18)$$

where k is Boltzmann constant and T temperature.

In more intensive electric fields the dipole moment μ grows slower and asymptotically come to saturated value, which corresponds to ideal arrangement of all

dipoles in the direction of electric field.

If a volume unit V consists of N molecules, the vector of polarization P will be given by

$$P = \frac{1}{V}\sum_{i=1}^{N}\mu_i + P_\infty = \frac{N}{V}\langle\mu\rangle + P_\infty \qquad (19)$$

where N denotes the number of all dipoles in the system and P_∞ is the contribution of induced polarization. Importance of dielectric spectroscopy lies in possibility to establish relations between structural parameters (μ_i, A_i,) and macroscopic value of P. It is known that the polarization vector P is given by macroscopic intensity of electrical field E (or electrical induction D) and material functions such as permittivity ε or susceptibility κ [33]. For corresponding interrelations the following equations are valid

$$P = \varepsilon_0 \kappa E \qquad (20)$$

$$P = D - \varepsilon_0 E = (\varepsilon - \varepsilon_0)E \qquad (21)$$

and

$$\varepsilon_0 \kappa = \varepsilon - \varepsilon_0 \qquad (22)$$

where ε_0 is the permittivity of vacuum ($\varepsilon_0 = 8.85 \cdot 10^{-12}$ F·m^{-1}). For practical reasons it is traditional to use the relative permittivity ε_r defined by equation:

$$\varepsilon_r = \frac{\varepsilon}{\varepsilon_0} \qquad (23)$$

Material functions susceptibility κ and permittivity ε have scalar character only in the case of isotropic dielectrics. In non-isotropic materials they are tensors.

2.3.2 Dynamic measurements

One of the most important applications of the dielectric spectroscopy is the study of relaxation processes which are caused by rotational/vibrational fluctuations of permanent molecular dipoles in time oscillating electric fields E^*. Such permanent dipols are related to characteristic parts of a molecule (fluctuation groups etc.) or to the

molecule as the whole. So we can obtain information about the dynamics of a molecular movement in a broad time (or frequency) range; the effect of external parameters such as temperature, pressure and composition of samples, etc., can be also investigated. The dielectric spectroscopy is (alike as in the case of stationary electric fields) based on the interaction of external electric field with matter. For small intensity fields E^* strengths D^* can be expressed by (see eqs (20- 22)) $D^* = \varepsilon^* \varepsilon_0 E^*$,where ε_0 is the dielectric permittivity of vacuum and ε^* is the complex dielectric function – dielectric permittivity. $\varepsilon^*$is a material value that is time (or frequency) dependent if time dependent processes proceed in measured samples. For a periodical electric field ($E(t) = E_0 e^{-i\omega t}$ (ω is the angular frequency) the complex dielectric function ε^* is given by

$$\varepsilon^*(\omega) = \varepsilon'(\omega) - i\varepsilon''(\omega) \qquad (24)$$

where $\varepsilon'(\omega)$ is the real part and $\varepsilon''(\omega)$ the imaginary part of the complex permittivity.

The simplest way how to calculate the time dependence of dielectric permittivity is the Debye's assumption that the rate of change of the *D(t)* is proportional to its value at time *t*

$$\frac{dD(t)}{dt} = -\frac{1}{\tau_0} D(t) \qquad (25)$$

where τ_0 is a characteristic relaxation time – time at which the value of *D* decreases to 1/*e*. For the complex dielectric function $\varepsilon^*(\omega)$ we obtain in this case [32-38]

$$\varepsilon^*(\omega) = \varepsilon_\infty + \frac{\Delta\varepsilon}{1 + i\omega\tau_0} \qquad (26)$$

The first term on the right-hand side of eq.(26), ε_∞, corresponds to the very high frequency response of material to the applied electric field *E* which is usually due to induced polarization and it is related to the refractive index ($\varepsilon_\infty = n^2$). In the limit of very low frequencies the permittivity corresponds to its static value (lim ε ($\omega \rightarrow 0$) = ε_s). With increasing frequency ω the real part $\varepsilon'(\omega)$ decreases stepwise from its static (relaxed) value ε_s to the un-relaxed ε_∞ ones whereas the imaginary part $\varepsilon''(\omega)$ exhibits for frequency $\omega_m = 1/\tau$ a maximum (Fig. 6). The position of maximum of imaginary part

agrees with the middle of the step in the real part. In limits of very low and very high frequencies the imaginary part of permittivity tends to zero. The difference of the real parts of permittivity limits $\Delta\varepsilon = \varepsilon_s - \varepsilon_\infty$ is called the dielectric strength or magnitude of absorption. Since both *ε'(ω)* and *ε"(ω)* are interrelated by the Kramers-Kronig relations

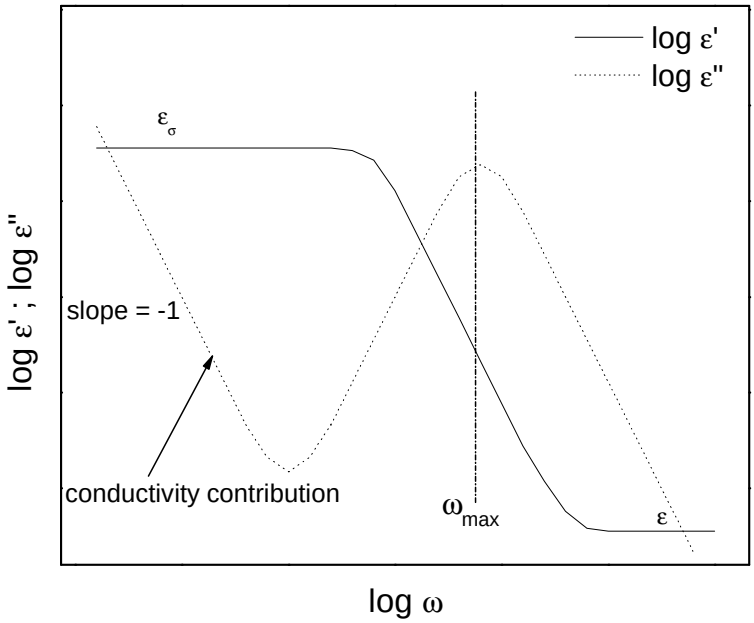

Fig. 6. *Scheme of real and imaginary part of the complex dielectric function for a relaxation process*

[34-35], both components of complex permittivity give roughly same information's about molecular motion. These relations are often used to relate the real and imaginary parts of response functions in physical systems.

Non-conductive materials - dielectrics - contain still a lot of charges that can move freely in external electric field and contribute to their direct-current (DC) conductivity σ_0. This DC conductivity contributes to the imaginary part of permittivity at low frequencies by the term

$$\varepsilon'' = \sigma_0/\omega \qquad (27)$$

In the case of dominating DC conductivity the experimental data may be evaluated not only by means of *ε** but also by complex conductivity *σ** (*σ*(ω) = iωε₀ε*(ω)*) or by complex modulus *M** (*M* = 1/ε**). The possibility of even small movement of charges in the external electrical field can lead to their separation which gives rise to an additional

polarization, so called Maxwell-Wagner-Sillars polarization or electrode polarization [15].

The equation (26) gives an adequate description of orientation polarization in the case of small concentrations of dipole moments when the dipole-dipole interaction is negligible (gases or diluted liquids). For all other materials including polymers we observe deviations from this Debye-like behavior concerning mainly the shape of experimental curves that are broader than Debye's ones. Therefore we suppose that the relaxation process is described by a set of different relaxation times and the frequency dependence of permittivity will be described by means of distribution function of relaxation times. In the literature there exist quite a number of empirical distribution functions for description of frequency dependences of dielectric relaxations. For evaluation of experimental results the non-symmetrical Havriliak-Negami empirical equation (see eq. (35)) is mostly used [36-38]. In many cases a more simpler - symmetrical Cole-Cole distribution, describes well experimental dependences of dielectric functions on frequency.

2.3.3 Dielectric measurements of polymer systems

a) amorphous polymers

The dielectric spectroscopy is a useful tool for study of molecular dynamics in polymer systems as it was shown in literature [37-38]. The molecular motions in amorphous polymeric systems could appear in different time (frequency) scales depending on the morphology of polymers. In most amorphous polymers there exist a number of relaxations corresponding to various kinds of molecular movements. Stockmayer [39,40] has divided the dipole moments in polymers in respect to the direction of the main-chain as A, B and C. Type A represents a part of dipole moment parallel to the main-chain. B-type dipole moment is perpendicular to the main-chain direction and type C represents dipole moments located in side-chains. At the lowest temperatures (glassy-state) or at the highest frequencies the secondary relaxations (γ-, β-relaxations) caused by local movements of molecular dipoles (the local rotational fluctuations or side-chain polar groups movement – type C) are usually detected. The temperature dependence of peak frequency f_m of these relaxations is usually described by the Arrhenius equation in the form of eq. (37). The magnitude of secondary relaxations is rather small and slightly increases with temperature. The shape of relaxations is broad

and approximately symmetric (Cole-Cole distribution).

With the increasing temperature the main relaxation referred to as the α-relaxation, corresponding to the main transition of polymer from the glassy to the rubbery state, is found. The movement in this region has a cooperative character. The temperature dependence of the relaxation times in the main transition region (temperature dependence of f_m) can be expressed by the Vogel-Fulcher-Tammann equation (eq. (38)) or by the equivalent Williams-Landel-Ferry equation (eqs (10), (11) and (13)). The dielectric strength in the main transition region is much higher than that of secondary relaxations; its value decreases with increasing temperature. The shape of main transition absorption peak is un-symmetric, corresponding to the Havriliak-Negami distribution (eq. (28)). Bauer and Stockmayer [39-40] have dielectrically measured poly(oxypropylen)-diols (PPD) and -triols (PPT) at which the A-type of dipoles is present. At the temperatures higher then the T_g they have found at lower frequencies than the α-relaxation a separate, so-called normal mode relaxation (α'-relaxation), which corresponds to the movement of the whole chain. While for the segmental α-relaxation the temperature position of maxima is practically independent of molecular weight M for measured diols and triols, for normal mode relaxation it depends on the length of molecule. It was shown that the peak frequency f_{m2} of normal mode depends on the molecular weight as

$$f_{m2} \propto M^{-A} \qquad (28)$$

where A ~ 3 for experimental data which were found at T = 220 K. The dielectric strength of normal mode relaxation depends also on the molecular weight of polymer because the dipole moment component is parallel to the chain backbone. The shape of normal mode is well described by the Davidson-Cole or Cole-Cole distribution.

b) side-chain LC polymers (SCLCPs)

In SCLCPs the mesogens are usually decoupled from the main-chain by a flexible spacer, which is made from aliphatic segments. The molecular dynamic in these systems is a result of complicated interplay between the polymer backbone and the liquid crystalline moieties in different mesophases. The overall molecular dynamic is characterized by several relaxation processes (Fig. 7).

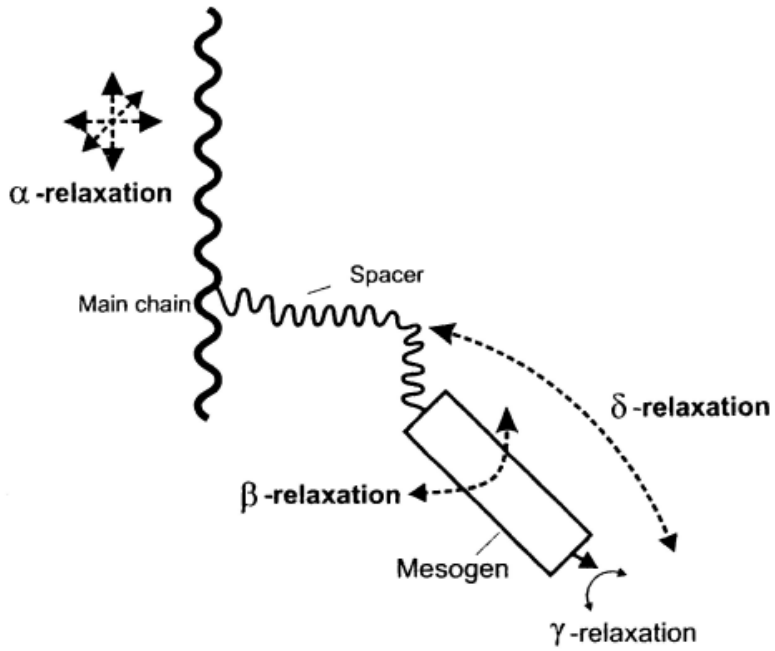

Fig. 7. *Scheme of liquid crystalline side-chain polymers. Possible dielectric relaxation processes are indicated by arrows (by Kremer and coworkers [15])*

The β-relaxation corresponds to libration fluctuations of the mesogen around the long molecular axis as proven by both the dielectric and NMR studies [41-44]. This β-relaxation should not be mixed up with the general nomenclature in amorphous systems, where β-relaxation simple means some secondary relaxation. The temperature dependence of peak frequency f_m of this relaxation is Arrhenius-like. Details of the structure of the mesogenic groups or of the main-chain have only a weak influence on its libration dynamics. Analysis of the activation energy E_a of β-relaxation, using the Arrhenius equation (eq. (37)), of various LCPs has led to extraordinary high E_a values which increased with the order in the mesophase in which relaxation was measured [15].

The α-relaxation is assigned to fluctuations of segments of the main polymer chain as in the case of amorphous polymers. This kind of relaxation shows a VFT-like (eq. (38)) dependence of f_m on temperature. It was shown that the local concentration of stiff moieties in the neighborhood of the main-chain segments is reduced resulting in an increased segmental mobility and hence in a decrease of T_g. [45]. The Vogel temperature T_{VFT} (eq. (38)) obtained from dielectric data correlates well with the glass transition temperature measured by calorimetric methods. The dielectric strength $\Delta\varepsilon$ of the α-relaxation shows a temperature dependence which is characteristic for the dynamic glass transition of amorphous polymers with no interruption at LC transitions.

In contrast to the α-relaxation the δ-relaxation behaves different. $\Delta\varepsilon$ is constant in the isotropic phase but decreases with decreasing temperature in the nematic phase. The

δ-relaxation is assigned to libration fluctuations of the mesogen around the short molecular axis. As a process originating from fluctuations of the mesogen and depending on the microviscosity of its surrounding, the δ-relaxation reflects the interplay between mesogens and the main polymer chain.

In addition to above relaxations other processes like a γ-relaxation (detected at the lowest temperatures) are related to rotational fluctuations of the tail or terminal groups of side-chains and are similar to those in amorphous polymers.

2.3.4 Free volume interpretation

The mechanism of segmental relaxation involves main-chain motion over large length scales. This intramolecular cooperativity requires intermolecular interaction, which might be represented in the description by the parameter of free volume similarly to mechanical relaxation.

Zorn and co-workers [46] transformed the Vogel-Fulcher-Tamman equation (38) to Williams-Landel-Ferry equation (11). Finally they came to

$$C_1^0 = \frac{1}{2.3} \cdot \frac{B}{T_0 - T_{VFT}} \tag{29}$$

and

$$C_2^0 = T_0 - T_{VFT} \tag{30}$$

The reference temperature T_0 in the WLF equation is based on an arbitrary choice of superposition-reference temperature and constants C_1^0 and C_2^0 depends on T_0. If we choose as the reference temperature the glass transition temperature T_g., then, according to the free volume theory (see 2.2.4), the fractional free volume f_g and the thermal expansion coefficient of the free volume α_f:

$$f_g = \frac{1}{2.3 C_1^g} \tag{31}$$

and

$$\alpha_f = \frac{1}{2.3 \cdot C_1^g \cdot C_2^g} \tag{32}$$

usually attain the universal values (f_g = 0.025 and α_f = 4.8 10^{-4} K^{-1})

2.4 Macroscopic structure characterization

2.4.1 Differential scanning calorimetry (DSC)

For investigation of various structural changes the differential scanning calorimetry (DCS) method is mostly used in literature. Method consists in the measurement of the specific heat c_p of the sample in dependence on temperature. While the first-order structural change (i.e. crystallization) gives a pronounced maximum in temperature dependence of c_p, the glass-transition in polymers leads to jump-wise temperature change of c_p. The essential features of the phase behavior of LCPs (including of SCLCPs) are relatively well established [47]. Most of LC polymers are non-crystalline in character: the differential scanning calorimetry (DCS) traces exhibit a glass transition associated with the movement of the polymer backbone and a first-order transition from the mesophase to the isotropic phase due to the presence of mesogens in main or side-chains. It should be pointed out that if sufficiently long flexible spacers are present in the structure partial crystallization of the main or side-chains may occur [47-48].

The transition temperatures are dependent on the sample history and molecular weight, so polymer samples must be heat-treated in the same manner and should be of sufficiently high molecular weight. It has been shown that a fraction of amorphous material in LCPs may be present together with the mesophase and the relative amount of the two phases is changing with the thermal history [26]. In some cases, the isotropic melt can even be quenched in ice-water to give a fully amorphous glass [41]. For such amorphous structures it has been found that the main transition temperatures T_g increases rapidly with molecular weight before leveling off; this has been discussed previously by many authors [19, 33, 35-50]. The shorter is the flexible spacer, the stronger is the temperature dependence of the T_g at low degrees of polymerization (low molecular weight of LC polymers).

2.4.2 Wide-angle X-ray scattering

X-ray diffraction provides information's concerning the arrangement and mode of packing of molecules and the type of order present in a ordered mesophase. For powder samples, the well-known Debye-Scherrer technique is usually used [51]. This method

gives all reticular spacings between molecules but no information about spatial orientation. Thus, it is often but not always possible to distinguish between the nematic and smectic phases of liquid crystals. Reliable characterization of molecular arrays given by X-ray diffraction is possible only in the ordered, aligned samples [51]. Oriented specimens can be prepared by the quick cooling in a strong magnetic (electric) field from the isotropic liquid phase down into the nematic phase [52].

2.4.3 Optical microscopy

Polarizing optical microscopy is also often used for determination of ordering in LCPs. Using a microscope with crossed polarizer's the formation of various textures (nematic, smectic A or C etc.) in polymer can be determined at various temperatures. Usually texture formation temperatures depend on cooling/heating rate.

3. The Aim of the Thesis

As it was discussed previously, physical properties of many LC polymers (mainly with mesogens in backbone chain) have been already investigated [15,18,41]. Generally, LC mesophase (showing more ordered smectic or less ordered nematic structure phase) greatly affects the thermal and physical properties of LCPs. In fact, incorporation of proper mesogenic groups into side-chains of polymer backbone result in self-assembled materials in which the molecular dipole correlations are maximized and lead to highly polar structures. From such polymers, processable films could be developed for photonic, electrooptic and second harmonic generation in non-linear optics. Especially side-chains liquid crystalline polymers (SCLCPs) with azobenzene mesogenic groups in side-chains form a promising class of photochromic materials which can find many practical applications, especially in photonic.

In the Institute of Macromolecular Chemistry AS CR new SCLCPs based on polybutadiene (PB) main-chain were synthesized. Side-chain liquid crystalline polybutadienes (SCLCPBDs) were prepared by addition reaction of SH group of LC thiol with double bonds of butadiene monomer unit. Two types of LC thiols with different structure of mesogenic and end side groups were synthesized and grafted to polybutadiene backbone; for modification the telechelic polybutadiene-diol (PBD) was used. In such a way SCLCPBDs with comb-like structure were prepared with various initial molar ratios of thiol to double bonds of PBD. These SCLCPBDs can be in future used for preparation of linear or crosslinked LC polyurethanes (SCLCPUs) by the reaction of grafted SCLCPBDs with diisocyanates and triols. In this work we investigate:

(1) Relations between structure and physical properties of a side-chains liquid-crystalline polybutadiene-diols (SCLCPBDs) with the comb-like architecture prepared by addition reaction of LC thiol - 4´-[(6-thiohexyl)oxy]biphenyl-4-carbonitrile with the double bonds of telechelic HO-terminated polybutadiene (PBD). SCLCPBDs with various initial molar ratios of thiol to double bonds of PBD, R_0, in the range from 0.15 to 1, were investigated. Their thermal and physical properties were studied by differential scanning calorimetry, dynamic mechanical and the broad-band dielectric spectroscopy. The effect of degree of modification on structural changes and physical properties was determined.

(2) Physical properties of a comb-like SCLCPBDs with LC azobenzene moieties in the side-chain mesogens; SCLCPBDs were made by radical addition of 5-(4-{[4-(octyloxy)phenyl]azo]}phenoxy)pentane-1-thiol onto the double bonds of PBD with various initial molar ratios of thiol to double bonds (R_0 = 0.2 to 1). Thermal structural transitions in SCLCPBDs are investigated by DSC, WAXS and polarizing microscopy; the broad-band dielectric spectroscopy was used for investigation of molecular dynamics in these SCLCPBDs. As in previous case amount of bound thiol on physical behavior is specified. We believe that these systems, as well as linear polyurethanes and networks formed from these SCLCPBDs, will find optical applications. In fact one SCLCPBD with R_0 = 0.4 was already used in optical investigations at room temperature and promising results were found; paper dealing with this results was submitted for publication [16].

4. Methods of Measurements

4.1 Mechanical measurements

Dynamic mechanical measurements were performed with a Bohlin C-VOR apparatus with the parallel-plate geometry. Small-strain oscillatory shear measurements were performed in the frequency range f (= $\omega/2\pi$, where ω is angular frequency) from 0.05 to 50 Hz at various constant temperatures and frequency dependences of the storage G', loss G'' moduli and loss tangent tg $\delta = G''/G'$ were determined. Sample was placed between the plates of the rheometer and heated until an isotropic melt was obtained; after that sample was cooled down and measurements were carried out in temperature interval from -50 to 100 ^{o}C. Heating and subsequent cooling rate was 2 K/min.

Using frequency-temperature superposition of data the superimposed curves of reduced moduli $G'_p = G' \cdot b_T$, $G''_p = G'' \cdot b_T$ and loss tangent tg δ_p = tg δ vs. reduced frequency $f.a_T$ (where a_T is horizontal and b_T is vertical shift factor [27]) were obtained. The horizontal shift factor a_T was obtained mainly from superposition of the loss tangent (for tg δ no vertical shift is necessary).

4.2 Dielectric measurements

Dielectric measurements were carried out with a Schlumberger 1260 frequency-response analyzer with a Chelsea dielectric interface, in combination with the Quatro cryosystem of Novocontrol. The samples were pressed between brass electrodes 15 mm in diameter with a spacing of 55 μm, maintained by silica fibers. The dielectric permittivity

$$\varepsilon^*(f) = \varepsilon'(f) - i\varepsilon''(f) \qquad (33)$$

where f is frequency, ε' is the real (storage) and ε'' is the imaginary (loss) component, $i = \sqrt{-1}$, was measured in the frequency range 10^{-1}-10^{6} Hz at temperatures between -150 and 130 ^{0}C upon heating (after cooling the sample to -150 ^{o}C from the isotropic state at 140 ^{o}C).

The frequency dependence of the complex dielectric function $\varepsilon^*(f)$ originates from fluctuations of molecular dipoles and/or dipoles induced by the charge separation at boundary layers inside the material (Maxwell-Wagner-Sillars polarization, MWS) or between the material and electrodes (electrode polarization), and from the propagation of mobile charge carriers [53]. We suppose that overall dielectric function ε^* consists of the dipole contribution ε_d^* and of the conductivity contribution ε_c^*

$$\varepsilon^* = \varepsilon_d^* + \varepsilon_c^* \qquad (34)$$

The frequency dependence of the dipole contribution to the complex dielectric function, ε_d^*, is usually described by the non-symmetrical Havriliak–Negami empirical equation [54]

$$\varepsilon_{\mathrm{d}}^* = \varepsilon_\infty + \Delta\varepsilon/[1+\mathrm{i}(f/f_{\mathrm{r}})^a]^b \qquad (35)$$

with five, generally temperature-dependent parameters: high-frequency (unrelaxed) value of the real part of permittivity ε_∞, the relaxation strength $\Delta\varepsilon = \varepsilon_0 - \varepsilon_\infty$ (ε_0 being the relaxed low-frequency value of permittivity), frequency f_{r} corresponding to the most probable relaxation time τ_r ($2\pi f_r\tau_r = 1$) and two shape parameters a and b. The parameter f_{r} is related to the peak frequency f_{m} at which the loss component ε'' on frequency attains its maximum value accounting to the following equation

$$\left(\frac{f_{\mathrm{m}}}{f_{\mathrm{r}}}\right)^a = \frac{\sin\left(\frac{a\pi}{2(b+1)}\right)}{\sin\left(\frac{ab\pi}{2(b+1)}\right)} \qquad (36)$$

In the case of symmetrical Cole-Cole distribution ($b = 1$), the frequencies f_{r} and f_{m} are identical [54]. A computer program based on the Marquardt procedure [55] was developed for determination of all parameters from the frequency dependence of ε'' at various temperatures.

The temperature dependence of frequency f_{m} could be described either by the Arrhenius equation

$$f_{\mathrm{m}} = f_{\infty} \exp(E_{\mathrm{a}} / kT) \qquad (37)$$

where E_a is the activation energy and f_{∞} is the pre-exponential frequency factor, or by the Vogel-Fulcher-Tammann equation (VFT) [12,53]:

$$\log f_{\mathrm{m}} = \log f_{\infty} - \frac{B}{T - T_{VFT}} \qquad (38)$$

where B is the apparent activation energy, f_{∞} the pre-exponential frequency factor, and T_{VFT} is the Vogel temperature (T_{VFT} ~ T_{g} - 50 °C, where T_{g} is the glass transition temperature).

The frequency dependence of the conductivity contribution to the complex dielectric permittivity, ε_c^*, can be described by the following equation [53]

$$\varepsilon_c^* = (i\frac{f}{f_0})^{\eta} \qquad (39)$$

where f_0 is an adjustable parameter and the exponent η would have the value -1 in the ideal case of pure time-independent DC conductivity.

The frequency dependence of the complex conductivity $\sigma^*(f)$ is given by the equation [53]

$$\sigma^*(f) = \mathrm{i}2\pi f\varepsilon_{\circ}\varepsilon^*(f) \qquad (40)$$

The complex electric modulus $M^*(f)$

$$M^*(f) = \frac{1}{\varepsilon^*(f)} \qquad (41)$$

is often used as alternative representation when emphasis is put on the charge carriers transport [15,53].

4.3 DSC measurements

Diferential Scanning Calorimetry measurements were carried out by Perkin-Elmer Pyris-1 equipment using the 10 K/min heating and cooling rate. From DSC traces the glass transition temperature, T_g, and LC/isotropic or different mesomorphic states transition temperatures, T_{mi}, were determined.

4.4 WAXS

Wide-angle X-ray diffractograms were measured on a HZG4A diffractometer (Freiberger Präzisionsmechanik, Germany) using Ni-filtered CuKα radiation. For high-temperature measurements a heating chamber with thermal stability of 0.5 °C was attached.

4.5 Optical measurements

The texture of crystalline and LC phases was determined by a polarizing optical microscope (Nicon Eclipse 80i, crossed polarizer's) equipped with a heating stage. The heating/cooling rate was 3 K/min.

5. Results and Discussion

5.1 Synthesis, structure, thermal, dynamic mechanical and dielectric behavior of liquid crystalline polybutadiene-diols with cyanobiphenyl mesogenic groups in side-chains

5.1.1 Synthesis of thiol and SCLCPBDs

The telechelic OH-terminated polybutadiene - Krasol LBH 3000 (PBD) (Kaučuk Kralupy, M_n~2400, 60 mole % of 1,2 and 40 mole % of 1,4 monomer units, number-average functionality f_n=2) of the structure

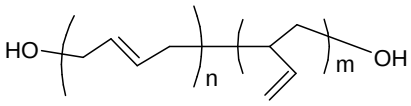

PBD was purified by addition of silica gel SILPEARL (Glass works Kavalier). Silica gel was repeatedly washed with deionized water, then its stirred suspension was boiled in water for 3 min and silica gel was filtered off. It was placed in an oven and heated to 160 – 180 °C under nitrogen atmosphere for 24 h. After cooling down to ambient temperature the activated silica gel was used to remove the antioxidant (Irganox 1520). 20 g of PBD was dissolved in 100 ml of benzene (dried over Na) and 5 g of activated silica gel was added to the solution. The reaction mixture was stirred at ambient temperature under N_2 atmosphere for 6 h. Then SiO_2 was filtered off, solvent was removed on a rotavapor and PBD was dried to constant weight (50 ^oC/ 6.7 Pa).

Materials for synthesis of thiol - 4´-hydroxybiphenyl-4-carbonitrile (Aldrich), 1,6-dibromohexane (Fluka) and thiourea (Fluka) were used as received.

Synthesis of *4'-[(6-bromohexyl)oxy]biphenyl-4-carbonitrile:* 25 g (0.128 mol) of 4-hydroxy-4-biphenyl-1-carbonitrile was dissolved in 660 ml of ethanol. Then 8.55 g (0.152 mol) of KOH in 66 ml of ethanol and 171 ml (0.044 mol) of 1,6-dibromohexane were added to the solution under nitrogen atmosphere. The reaction mixture was stirred at 75 ^oC for 6 h. After cooling, the precipitate (NaBr) was filtered off and ethanol was removed on a rotavapor. The residual oil was dissolved in diethyl ether and the solution was purified by addition of silica gel. The silica gel was filtered off and the filtrate was

poured into methanol. The precipitated product was dried and purified by precipitation from diethyl ether with methanol: m.p. 63-65 ^{o}C. Yield: 40.17 g (88 %).

Synthesis of *4´-[(6-thiohexyl)oxy]biphenyl-4-carbonitrile(TH1):* A mixture of 40.17 g (0.112 mol) of 4´-[(6-bromohexyl)oxy]biphenyl-4-carbonitrile and 8.73 g (0.113 mol) of thiourea in 400 ml of absolute ethanol was heated at 80 ^{o}C for 20 h. Then the reaction mixture was cooled to room temperature and concentrated on a rotavapor. The obtained thiuronium salt was filtered off and recrystallized from absolute ethanol; m.p. 168-170 ^{o}C. Yield 46.95 g (96.4 %). 2.6 g (0.006 mol) of the salt was hydrolysed with 0.45g (0.008 mol) of KOH in ethanol/water mixture (2/20 ml) by refluxing under nitrogen atmosphere for 7 h. After cooling to room temperature the potassium thiolate was acidified with 1 ml of acetic acid. Ethanol was then evaporated under vacuum and the crude thiol was isolated by extraction with chloroform. Chloroform solution was extracted with water and dried over anhydrous calcium chloride. The solvent was evaporated on a rotavapor to give the product; m.p. 49-51 ^{o}C. Yield: 1.72 g (92.3%). The synthesized LC thiol TH1, with mesogenic group in the side-chain, of the structure:

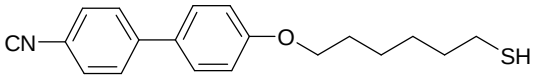

TH1

was used in addition reaction of the terminal thiol group with double bonds of PBD.

LCPBDs: In radical addition of TH1 onto double bonds of PBD 2,2'-azobis(2-methylpropanonitrile) (AIBN) was used as a initiator; the reaction proceeded in toluene solution (54 g of PBD in 1 l of toluene) at the initiator-to-thiol ratio 5x10^{-2} mol at 60 °C for 48 h. We have synthesized SCLCPBDs with various initial molar ratios of thiols to double bonds of PBD, R_0, in the range from 0 to 1. The structure of SCLCPBDs is as follows:

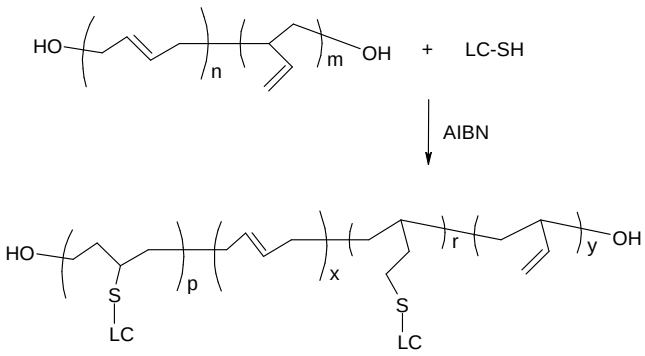

5.1.2 Characterization of SCLCPBDs: elemental analysis, NMR spectroscopy and GPC

The experimental degree of modification, R_{eS} ([bound thiols]/[double bonds]), after the addition and purification, was determined from elemental analysis using the relation

$$R_{eS} = 32 \times w_S / (54 + 311.5 \times w_S) \qquad (42)$$

where w_S is the weight fraction of sulfur bounded in SCLCPBDs determined by elemental analysis (Table 1).

The degrees of modification were determined also by ^{1}H and ^{13}C NMR spectroscopy (300.1 MHz and 75 MHz, respectively, 60 °C. For R_{eNMR} determination the integrated intensity of the signal of OCH_2 LC-thiol protons at 4.0 ppm (or signal of aromatic protons) was used. In this case the detailed structure of SCLCPBDs (amount of 1,2 and 1,4 butadiene units [56], hydrogenated BD monomers and end OH groups [57]) could be evaluated.

The number- (M_n) and weight-average (M_w) molecular weights were determined by GPC (modular LC system with refractive index detection, column 30×8 SDV 10000) calibrated with PS standards. THF was used as solvent and measurements were carried out at ambient temperature.

5.1.3 Structure and degree of SCLCPBDs modification

As follows from Fig. 8, two peaks gradually appear in GPC chromatograms with increasing initial ratio of thiols to double bonds, R_0. The increase in number-average (M_n) and weight-average (M_w) molecular weights corresponding to individual peaks and to their sum with R_0 is shown in Fig. 9. These results suggest that the addition reaction leads to bimodal molecular weight distribution at all degrees of modification. From Fig. 9a it follows that even at the lowest R_0 (0.15) both peaks persists; M_n ~ 10000, found for the low-molecular-weight peak, practically does not change with increasing R_0. The increase in the modification rate, observed in Fig. 9b for total molecular weight averages at R_0 ~ 0.5 suggests that the bimodal distribution is probably associated with different rates of the

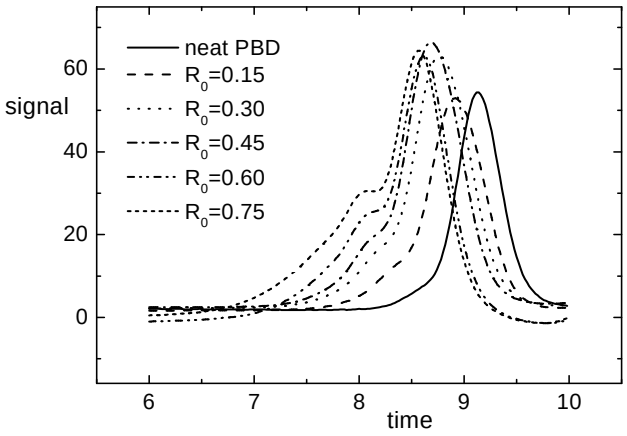

Fig. 8. *GPC chromatograms for neat PBD and modified SCLCPBDs (R_0 = 0-1.0)*

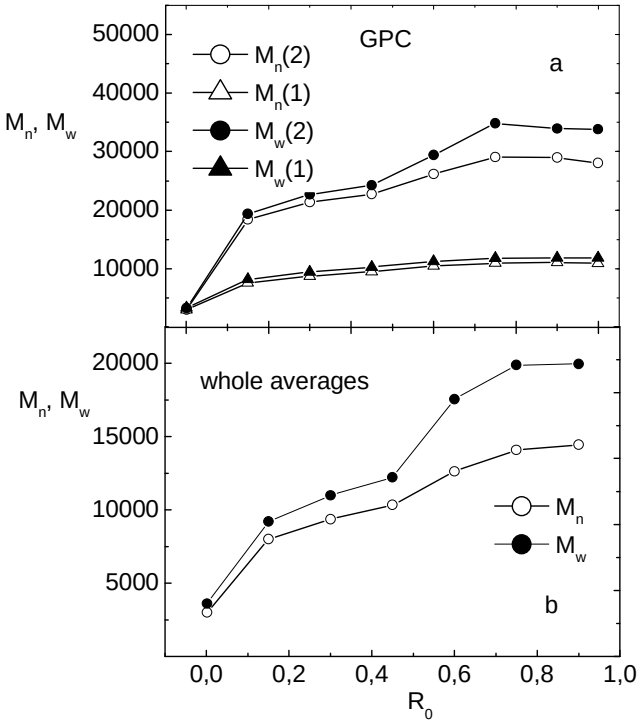

Fig. 9. *Number- (M_n) and weight- (M_w) average of molecular weights of individual peaks of neat PBD and modified SCLCPBDs*

addition of SH group on 1,2 and 1,4 double bonds of PBD. From Fig. 9b one can also see that for $R_0 > 0.5$ polydispersity of the systems (the ratio M_w/M_n) increases.

Comparison of various experimental degrees of modification, obtained from GPC, R_{eGPC}, (from total number-average M_n), weight fraction of sulfur, R_{eS} and NMR analysis, R_{eNMR} in dependence on initial ratio R_0 is shown in Fig. 10. As expected, the modification

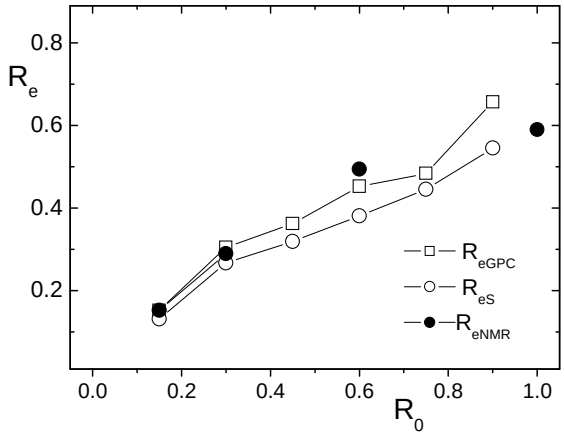

Fig. 10. *Experimental degree of modification R_e: from S content - R_{eS}, from GPC - R_{eGPC} and from ^{1}H NMR -R_{eNMR} in dependence on initial ratio of thiols/double bonds - R_0*

degrees, determined by all three methods, increase with increasing R_0; the values determined from the GPC and NMR are slightly higher than those determined from sulfur analysis. While for the lowest initial thiol contents R_0 ($R_0 \leq 0.3$), $R_0 \sim R_{eS}$, for higher R_0, $R_{eS} < R_0$ was found. Substantially lower R_{eS} values suggest that at the highest R_0 values steric hindrances probably prevents the addition. We believe that also the dimerization reaction of thiols can take place in presence of initiator by recombination of THS radicals. ^{1}H NMR spectroscopic measurements show that with increasing R_0, in addition to PB units grafted with thiols, some amount (x_H) of hydrogenated-like units (without double bonds) in SCLCPBDs are formed. While for neat PBD amount of hydrogenated-like units $x_H \sim 0$, after modification with $R_0 = 0.75$, $x_H \sim 0.14$. It is interesting to notice that the highest experimental R_{eS} value roughly correlates with amount of 1,2 monomer units in PBD. ^{1}H and ^{13}C NMR spectroscopy also proved that the functionality (concentration of OH groups) of SCLCPBDs does not change with the extent of the addition reaction.

5.1.4 Thermal behavior

An example of DSC traces of neat thiol and SCLCPBD with R_{eS} = 0.51 (R_0 = 1.00) is shown in Fig. 11; the corresponding transition temperatures determined from DSC data on cooling (C) and subsequent heating (H) scans are summarized in Table 1.

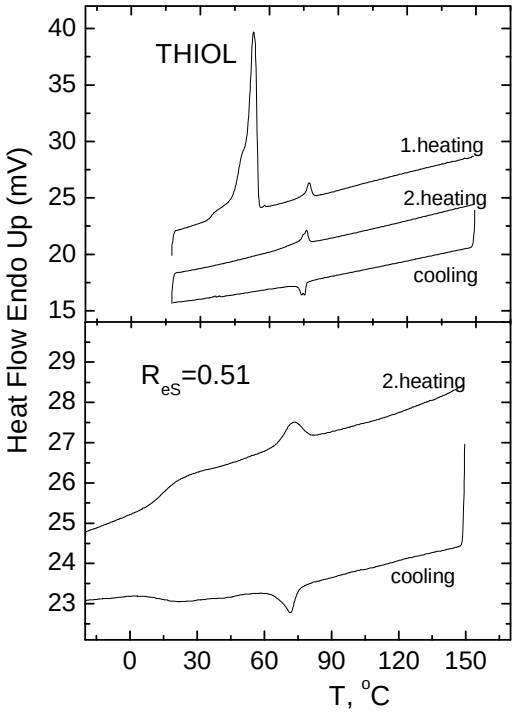

Fig. 11. *Example of measured DSC traces for neat TH1 and SCLCPBDs with R_{eS} = 0.51 (R_0 = 1.0). Cooling and heating rate was 10 K/min*

After synthesis and purification the TH1 was a crystalline powder; on the first heating the melting of crystalline phase was observed at temperature T_m = 53 °C (ΔH_m ~ 59.6 J/g) followed by second endotherm – melting of the mesophase at 77.4 °C (ΔH_m ~ 3.6 J/g). On subsequent cooling and second heating only formation and melting of mesophase takes place at T_m ~ 76 °C (ΔH_m ~ 3.4 J/g). As expected, simple amorphous behavior with only the glass transition was found for neat PBD and the polymer with the lowest R_{eS} value; the changes in the specific heat ΔC_p ~ 0.45 J/g.K have the values typical of amorphous polymers [27] (Table 1). With increasing R_{eS} the glass transition temperature of SCLCPBDs increases from ~ -46 °C (neat PBD) to 20 °C (R_{eS} ~ 0.51); at the same time the changes in the specific heat ΔC_p decrease. For $R_{eS} \geq 0.38$, both, the T_g and ΔC_p values are roughly constant, independent of the extent of modification. LC mesophase

Table 1. *Degree of modifications and DSC results of TH1, neat PBD and SCLCPBDs.*

R_0	R_{eS}.100	Run	T_g °C	ΔC_p J/g	T_m °C	ΔH_m J/g
TH1	0	H C			76.2 75.3	4.4 -4.3
PBD	0	H C	-47.3 -44.2	0.49 0.42		
0.15	13.1	H C	-13.2 -15.2	0.47 0.40		
0.30	26.7	H C	9.6 12.4	0.38 0.41	26.9	0.7
0.45	31.9	H C	14.6 11.4	0.36 0.24	48.9 42.3	3.2 -3.0
0.60	38.1	H C	20.1 18.3	0.39 0.24	62.7 59.2	3.7 -3.7
0.75	44.5	H C	21.3 19.7	0.34 0.24	68.4 65.7	3.8 -3.7
0.90	51.1	H C	18.7 17.6	0.34 0.23	73.2 71.8	4.1 -3.9
1.00	51.4	H C	20.0 19.0	0.32 0.20	74.4 72.9	5.5 -4.5

formation starts at R_{eS} ~ 0.27 (T_m ~ 27 °C). With increasing R_{eS}, the T_m increases and for R_{eS} ~ 0.51 reaches the value T_m ~ 74 °C which roughly corresponds to the T_m of neat thiol. With increasing modification also the change in the enthalpy ΔH_m at LC transition increases from 0.7 to 5.5 J/g. From the results shown in Fig. 11 and Table 1 it follows that ordering of mesogenic side-chains is not much affected by their connection to BD main-chain in comparison with ordering of neat thiol.

5.1.5 Dynamic mechanical behavior

The temperature dependences of the storage modulus, G', and loss tangent, $tg\ \delta$ (measured at frequency f = 1 Hz), of neat PBD and selected SCLCPBDs are shown in Fig. 12.

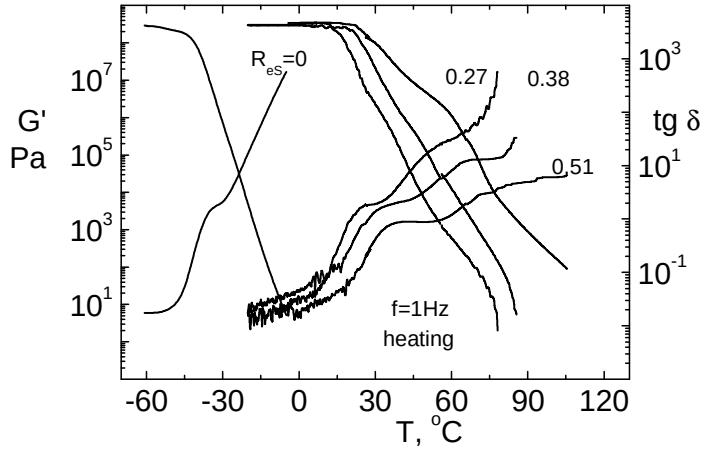

Fig. 12. *Temperature dependences of storage modulus G' and loss tangent tg δ measured at f = 1 Hz on heating at 2 K/min. R_{eS} values correspond to Table 1*

The pronounced decrease in the G' (more than 7 orders of magnitude) with temperature can be clearly seen. The glass transition is seen also on temperature dependences of the *tg δ* as a maximum located at the lowest temperatures. While at the highest temperatures the rubbery and flow behavior is observed (increase in *tg δ* with *T*), at the lowest temperatures the glassy state is reached with the highest values of storage modulus G', typical of the glassy state ($G' > 10^8$ Pa). With increasing modification of PBD (increasing R_{eS}), the changes in the position and shape of mechanical functions on temperature can be seen (Fig. 12). With increasing R_{eS}, the position of both mechanical functions shifts to higher temperatures and the height of the loss tangent maximum (*tg* δ_m) corresponding to the glass transition decreases. Only for neat PBD, expected liquid-like behavior at the highest temperatures is observed (strong increase in *tg δ* and decrease in G' with temperature); for modified SCLCPBDs additional, not well developed maximum in the *tg δ* on *T* dependence is seen at higher temperatures. The decrease in *tg* δ_m is associated with increasing amount of polymer chain units involved in the ordered state; at the same time, strong physical interactions between mesogens in the side-chains, which act as physical crosslinks, cause an additional maximum in the *tg δ* dependence at high temperatures.

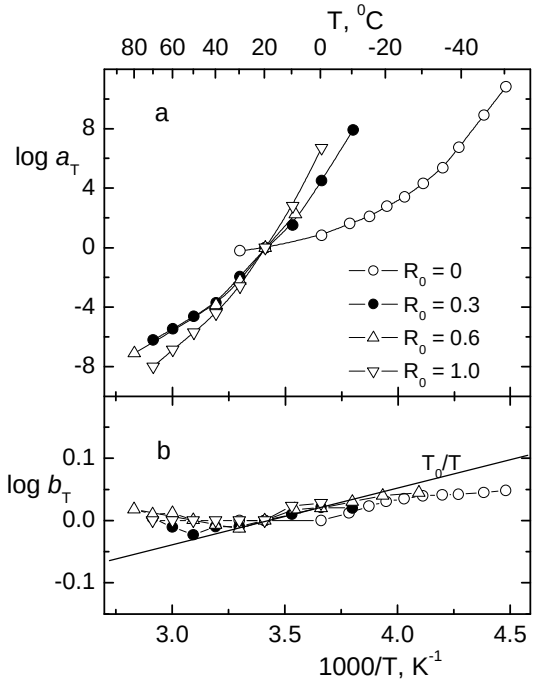

Fig. 13. *Temperature dependences of the horizontal a_T and vertical b_T shift factors at T_0 = 20 ºC. Curves are WLF dependences with C_1^0 and C_2^0 constants shown in Table 2*

As it was mentioned, we have applied the frequency-temperature superposition to dynamic mechanical functions measured in dependence on frequency at various constant temperatures. Due to small values of enthalpy found for mesophase transitions (Table 1) almost satisfactory superposition could be done for all measured polymers. The temperature dependences of the horizontal shift factors, log a_T, of all the polymers follow the WLF equation (eq. (11)) (Fig. 13a) with the reference temperature T_0 = 20 °C (Table 2).

Table 2*. Constants of WLF equation and free volume parameters*

R_0	C_1^0	C_2^0 K	f^0	$\alpha_f .10^4$ K^{-1}
0	6.89	123.6	0.063	5.1
0.30	14.65	65.5	0.030	4.5
0.60	17.52	80.6	0.025	3.1
1.00	25.08	104.8	0.017	1.6

From these constants the fractional free volume f^0 and the thermal expansion coefficient of the free volume α_f were calculated ($f^0 = 1/2.3\,C_1^0$ and $\alpha_f = 1/2.3\,C_1^0\,C_2^0$, Table 2),

respectively. As expected, the free volume value f^0 of neat PBD is the highest for the difference $T_0 - T_g \sim 65$ °C. For further three SCLCPBDs, $T_0 \sim T_g$ (Table 1) and f^0 values roughly correlate with expected universal value $f_g = 0.025$ [27]. It is interesting to mention that the expected universal value of α_f (= 4.8×10^{-4} K^{-1}), which does not depend on the reference temperature T_0, was found for neat PBD and polymer with $R_{eS} = 0.27$ ($R_0 = 0.3$); two polymers with higher R_{eS} values show substantially lower α_f values. We believe that also these unexpected low α_f values are due to strong side-chain interactions between mesogens. At the superposition we have used the vertical shift factor b_T shown in Fig. 13b; in this figure also theoretical dependence ($\log b_T \sim T_0/T$, [27]) is shown. It can be seen that experimental temperature dependences of $\log b_T$ are slightly lower than those theoretically expected. It is interesting to notice that in the region from 50 to 80 °C small increase in $\log b_T$ was found; in the same temperature region melting of mesophase takes place (Table 1).

The detailed dependences of superimposed curves of storage G'_p and loss G''_p moduli as well as loss tangent tg δ on the reduced frequency $f \cdot a_T$ are shown in Fig. 14. As expected, with increasing modification the superimposed curves are shifted to lower frequencies; at the same time a broadening of the main transition region takes place. Most pronounced changes in the shape of superimposed curves are seen in the rubbery and flow regions (at the lowest frequencies). In this region the expected slopes of mechanical functions ($G'_p \sim (f \cdot a_T)^2$, $G''_p \sim (f \cdot a_T)^1$ and tg $\delta \sim (f \cdot a_T)^{-1}$) vs. $f \cdot a_T$) for Newtonian liquids [27,58] are found only for neat PBD (Fig. 14). For modified samples, due to strong side-chains interactions, Newtonian behavior is not reached and in this frequency region a contribution of an additional (slow) relaxation process occurs.

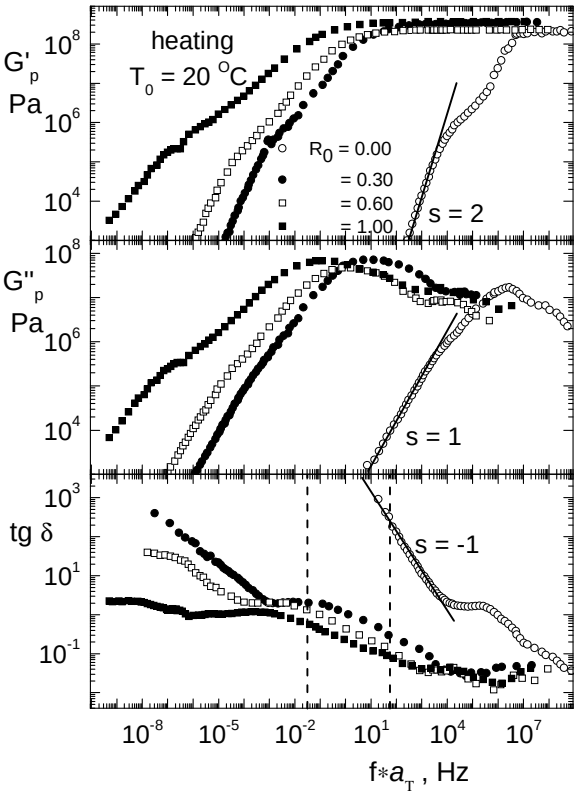

Fig. 14. *Frequency dependences of the superimposed storage G'_p, loss G''_p moduli and loss tangent tg δ, at reference temperature T_0 = 20 °C. The indicated slope values, s, are expected for Newtonian liquid mechanical behavior. Dashed lines show used frequency interval*

The magnitude of this process decreases with increasing modification; we believe that this process is associated with the movement of ordered chain clusters. With increasing R_{eS}, cluster sizes increase and the motion is more extensively hindered. It is interesting to note that the sample with the highest modification (R_0 = 1.0) roughly behaves as a system with critical gel (CG) structure in the gel point, for which independence of *tg* δ of frequency at the lowest frequencies is characteristic [58]. This would suggest that in this sample, due to strong mesogen interactions, a first infinite structure was formed and this structure is stable in the measured frequency and temperature region. This is in agreement with our preceding finding on ordered PU systems with mesogenic groups in the main-chain where we proved that CG structure was formed by a contribution of strong physical interactions as well as chemical junctions [59].

5.1.6 Dielectric behavior

It is well known that all glass-forming polymers exhibit primary relaxation – α; this relaxation is assigned to motion of polymer main-chain segments and is related to the glass transition (dynamic glass transition). The temperature dependence of its relaxation time is described by the Vogel-Fulcher-Tammann (VFT) equation (eq. (38)), which describes the slowing down of the relaxation approaching to the glass transition temperature. Besides the α-relaxation, usually additional (secondary) relaxations (β- or γ-relaxations) of faster time scales take place at lower temperatures. The β- and γ-processes generally occur in the glassy state, and have different molecular nature compared with the α-relaxation [15]. These secondary relaxations usually exhibit an Arrhenius temperature dependence of relaxation times (eq. (37)), in contrast to the much stronger VFT temperature dependence found for primary α-relaxation.

The overall dynamics in our side-chain liquid crystalline polymers is characterized by four dielectric relaxation processes, γ, β, α and δ, in the order of increasing temperature or decreasing frequency. The γ process is related to movement of the terminal (soft) groups of the side-chain, the β- relaxation corresponds to liberation fluctuations of mesogens around the long molecular axis and the α-relaxation is assigned to fluctuations of segments of the polymer main-chain (as observed in glass-forming systems). The δ-relaxation is assigned to liberation fluctuations of mesogens around the short molecular axis; presumably it is a rather multistep process with motional averaging rather than a 180 flip-flop jump of the mesogens [15, 60]. This process is probably associated with crystall/isotropic or LC/isotropic state transition.

The temperature dependences of the real (ε') and imaginary (ε'') parts of complex permitivity measured at frequency 1 Hz in cooling and subsequent heating regime in temperature range from –40°C up to 130°C for various degrees of SCLCPBDs modifications are shown in Fig. 15.

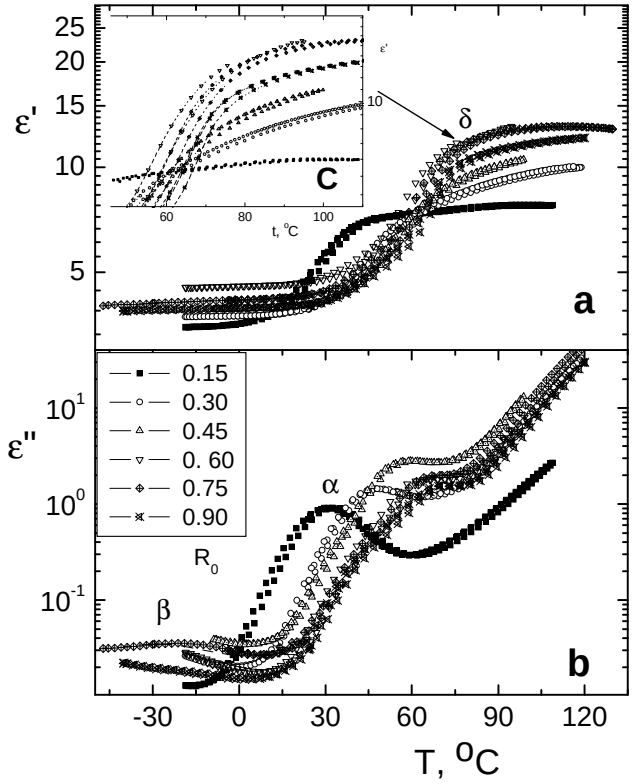

Fig. 15. *Temperature dependences of the real, ε΄, and imaginary, ε΄΄, parts of complex permittivity measured at frequency 1 Hz (cooling and heating rate was 2 K/min)*

The frequency dependences of both parts of complex permittivity for two selected temperatures (-60 °C and 70 °C) are shown in Fig. 16. With regard to low values and low changes of the ε' at temperature -60 °C its frequency dependence and decomposition is shown in detail in the inset of Fig. 16. From experimental data we could separate four relaxation regions labeled γ, β, α, δ (with increasing temperature). In the low temperature region two absorptions denoted as γ and β, which are associated with the local motion of 1,2 units of polybutadiene backbone (γ) and to the movement of mesogen along its long axis (β) were found. In the middle temperature region the main transition (α relaxation) was measured for all SCLCPBDs. At the highest temperatures, partly hidden under DC conductivity in the ε'' vs. f dependence, the δ-absorption, which is associated with the movement of mesogens along the short axis, was detected.

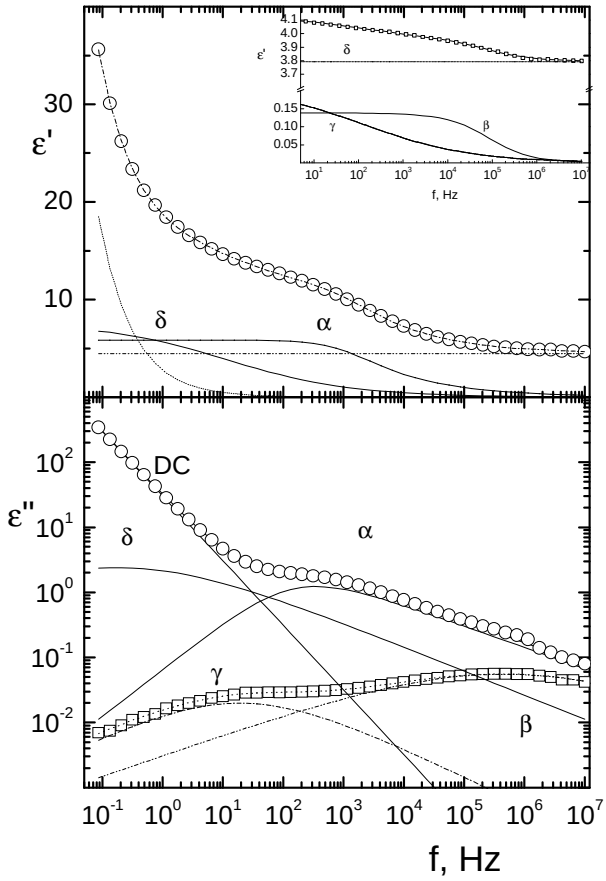

Fig. 16. *Frequency dependences of the the real, ε´, and imaginary, ε´´, parts of complex permittivity, measured at temperature T = -60 ^{o}C and 70 ^{o}C for sample modification with R_0 = 0.75. Symbols-experimental points, lines-corresponding decomposition to individual relaxation regions and DC conductivity*

An example of measured frequency dependences of the real and imaginary part of the dielectric permittivity, *ε'* and *ε"*, for the SCLCPBD with R_0 = 0.3 in the temperature range from 30 and 80 ^{o}C is shown in Fig. 17. A well-resolved peak, which shifts to higher frequencies with increasing temperature, can be observed. This peak corresponds to the main relaxation (α), which is associated with the cooperative motion of segments of PBD backbone chains and is related to its glass transition temperature determined by DSC and dynamic mechanical measurements.

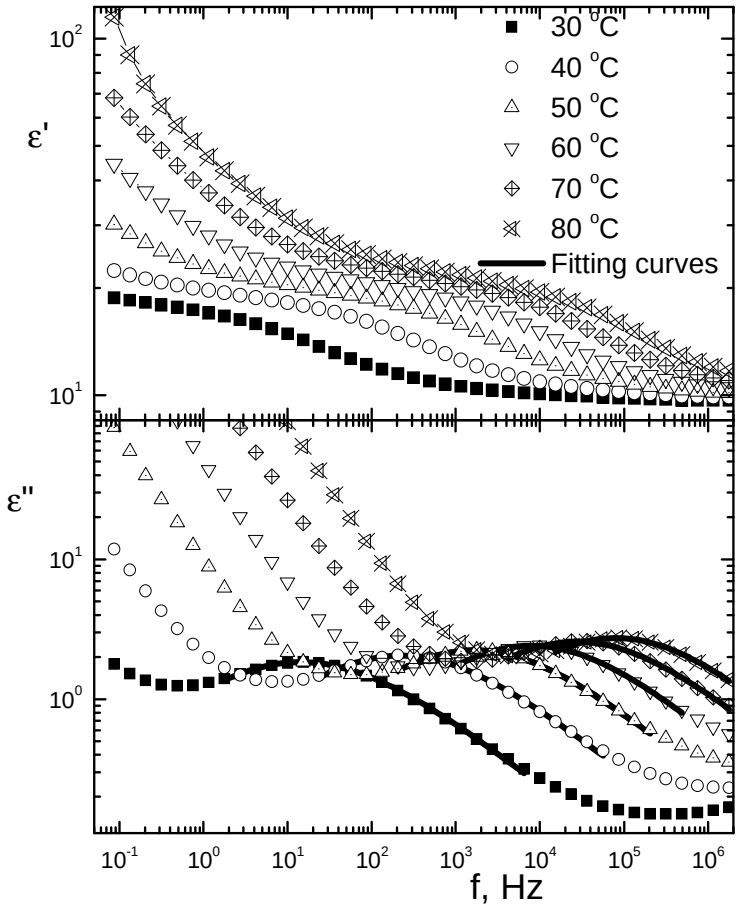

Fig. 17. *Frequency dependences of the real and imaginary part of the dielectric permittivity, ε' and ε", for the SCLCPBD with R_0 = 0.3 in the temperature range from 30 and 80 °C (region of the main α- relaxation). The numbers at curves denote temperatures in °C*

An another example of measured frequency dependences of the real and imaginary part of the dielectric permittivity, *ε'* and *ε"*, for the SCLCPBD with R_0 = 1 at the lowest temperatures is shown in Fig. 18. One can detect two processes – the first one (γ-relaxation) at the lowest temperatures at about -80 °C and the other one (β-relaxation) at higher temperatures. The relaxations assigned to the β-relaxation correspond to liberation fluctuations of the mesogens around their long molecular axis.

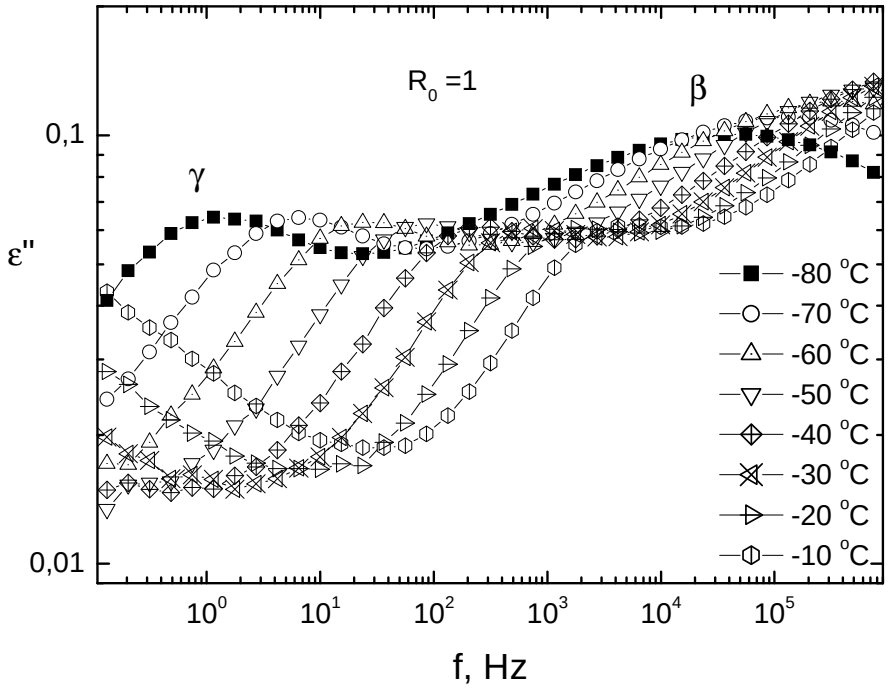

Fig. 18. *Frequency dependence of dielectric loss conductivity* ***ε"*** *at low temperatures*

Temperature dependences of absorption frequency peaks of the main transition region follow the WLF equation (eq. (10)) for all SCLCPBDs (Fig. 19); using this equation the characteristic temperatures T_S were calculated (Table 3). The T_S temperatures increase with increasing R_0 in accord with the increase of T_g temperatures determined by DSC (Table 1). On the other hand the temperature dependences

Table 3. *Degree of modification, DSC and dielectric results of* T_s, α_g *and* f_g.

R_0	R_e	T_g °C	T_s °C	$\alpha_f .10^4$ K^{-1}	f_g
0	0	-47.3	-10.5	4.0	0.092
0.15	0.13	-13.2	31.5	3.5	0.067
0.30	0.27	9.6	43.5	3.0	0.061
0.45	0.32	14.6	54.5	2.8	0.060
0.60	0.38	20.1	62	2.9	0.055
0.75	0.45	21.3	63	2.7	0.050
0.90	0.51	19.7	69	2.2	0.053
1.00	0.52	20.0	66	2.2	0.050

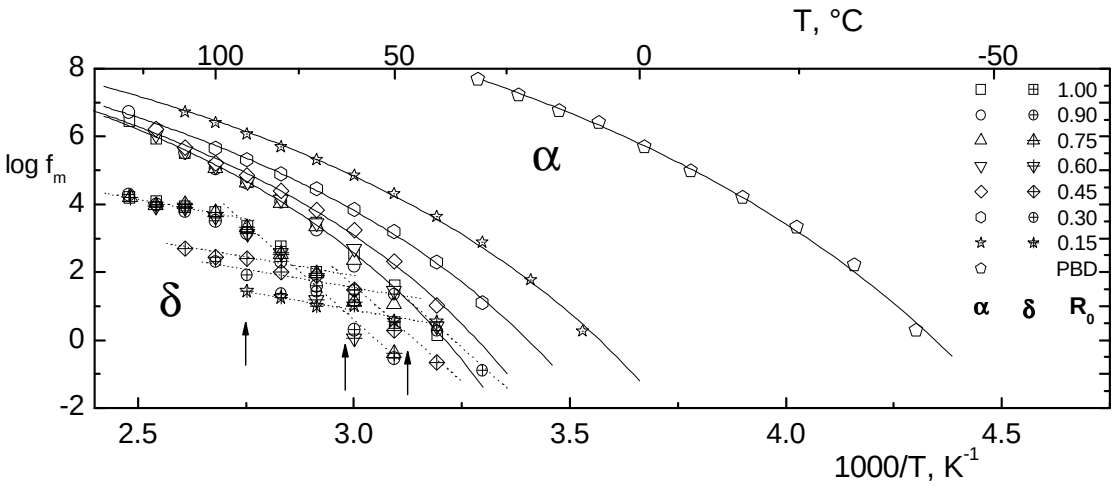

Fig. 19. *Temperature dependence of frequency peak maxima for α and δ transitions*

of absorption peaks were fitted by VFT equation (eq. (38)). Using eqs (29-32) from VFT parameters and T_g values determined by DSC the free volume characteristic - fractional free volume at T_g, f_g and thermal expansion coefficient α_f were calculated (Table 3). Both values decrease with increasing degree of modification, R_0. Similar decrease of these parameters was found from mechanical measurements (Table 2).

The magnitude of dielectric absorption in the main transition region $\Delta\varepsilon.T$ depends on the R_0 (Fig. 20). For low degrees of modification (R_e < 0.2) the magnitude increases and after that reaches roughly constant value ($\Delta\varepsilon.T$ ~ 2800K). This effect of saturation suggests that dipol-dipol interactions of mesogenic units and steric hindrances in PBD play decisive role.

Frequency shape of dielectric absorption in the main transition (α) region is for all modified samples asymmetric (Figs 16 and 17) and corresponds to the Havriliak-Negami distribution function with parameters a ~ 0.7 and b ~ 0.5. While the shape of the low-frequency part of SCLCPBDs curves practically does not change in comparison with PBD (a_{PBD}~0.69), the high frequency shape differs (b_{PBD} ~0.26). This means that the high frequency part of dielectric spectrum of modified samples is much narrower in comparison with neat PBD.

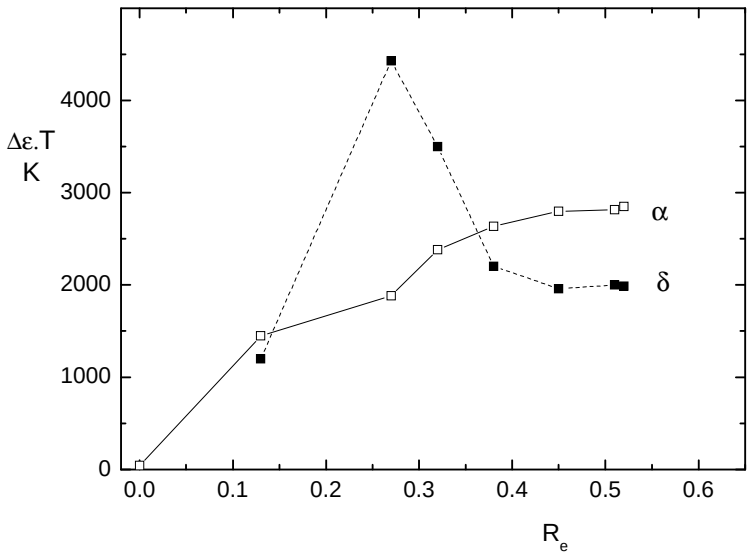

Fig. 20. *Dependence of magnitude $\Delta\varepsilon T$ on degree of modification R_0 for α and δ relaxations*

Frequency peak of the δ-absorption, corresponding to the motion of mesogen along its short axis, is shifted to higher temperatures with respect to the main transition region (Fig. 19). Since the size of mesogen is rather short its movement is closely linked up to the segmental movement of PBD chain. With regard to this, the separation of α and δ peaks was rather difficult. Nevertheless we could determine the change of activation energy at transition from LC to isotropic state as it was observed for other LCSC polymers.

As follows from Fig. 19 the temperature dependence of δ-absorption frquency peaks can be described by Arrhenius equation (eq. (37)) with two different activation energies. For sample with R_0 = 0.15 the value of activation energy was E_a ~ 0.45 eV in the whole measured temperature region. For all other modifications the change of activation energy from E_a ~ 0.45 eV (isotropic state) to E_a ~ 2.2 eV (LC state) was found. This is in agreement with DSC and mechanical measurements where the LC state was detected for SCLCPBDs except sample with R_0 = 0.15. Temperatures at which there are changes of E_a are shown in Fig. 19 marked by arrows; their shift to lower temperatures with decreasing R_e corresponds well to the shift of T_m measured by DSC (Table 1).

The magnitude $\Delta\varepsilon.T$ of δ-absorption is comparable to that of main transition, but it depends on temperature; with decreasing temperature the $\Delta\varepsilon.T$ decreases. The dependence of $\Delta\varepsilon.T$ on R_0 determined for LC transition is shown in Fig. 20. For first two R_0 values the $\Delta\varepsilon T$ increases and after that it decreases and reaches equilibrium value $\Delta\varepsilon T$ ~ 2000 K. Also this finding is in good agreement with main role of dipol-dipol interactions of mesogenic units and of steric hindrances in PBD. The shape of δ-

absorption is symmetric and rather broad in accord with the Cole-Cole distribution (a ~ 0.5 and b = 1).

The low temperature β-absorption peak was observed only for modified samples. The temperature peak position of absorption does not depend on R_0 value (Fig. 21) and follows Arrhenius equation (eq. (37)) with activation energy E_a ~ 0.55 eV. For R_0 < 0.5 the magnitude $\Delta\varepsilon T$ is roughly constant ($\Delta\varepsilon.T$ ~ 200 K); for higher R_0 decreases to $\Delta\varepsilon.T$ ~ 70 K (for R_0 = 0.90). The value of Cole-Cole a parameter increases with increasing temperature ($\Delta a/\Delta(1000/T)$ ~ -0.22 K) and for -30 ^{o}C a ~ 0.4 was detected. Since this absorption was not observed in neat PBD we believe that it is due to the motion of mesogens along their long axis.

The last measured γ-absorption was observed for all samples (including neat PBD). As in previous case its temperature position does not depend on R_0 (except neat PBD whose position on temperature scale is shifted to higher frequencies) (Fig. 21) and follows the Arrhenius equation with activation energy E_a ~ 0.4 eV. The shape of Cole-Cole parameter is the same as in previous case and exhibits weak dependence on temperature; for -30 ^{o}C a ~ 0.3 was found for all samples. The magnitude practically does not depend on R_0 and is $\Delta\varepsilon.T$ ~ 30 K. The γ-absorption measured for neat PBD has the

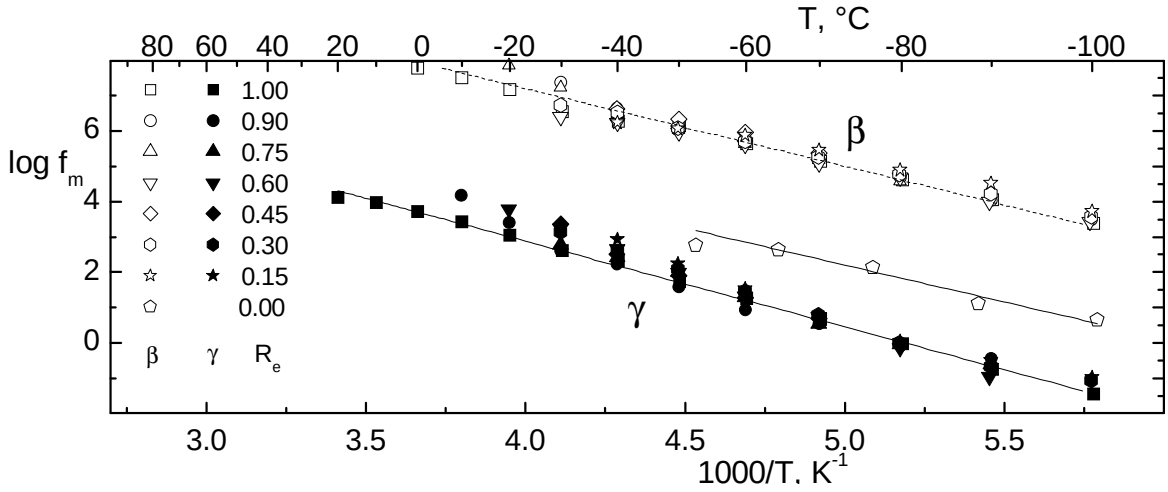

Fig. 21. *Temperature dependence of frequency peak maxima for β and γ transitions*

same values of E_a, $\Delta\varepsilon.T$ and a. From this fact we conclude that γ-absorption originates in local movement of 1,2 and 1,4 groups of PBD [63]. Detailed discussion of dielectric behavior of neat PBD will be given in section 5.2.

5.2 Synthesis, structure, thermal and dielectric behavior of liquid crystalline polybutadiene-diols with azobenzene mesogenic groups in side-chains

5.2.1 Synthesis of thiol and SCLCPBDs

The telechelic OH-terminated polybutadiene diol - Krasol LBH 3000 (PBD) (Kaučuk Kralupy, M_n~2400, 60 mol-% of 1,2 and 40 mol-% of 1,4 monomer units, number-average OH functionality f_n=2) was the same as previously used.

The synthesis of the LC thiol 5(4-[(4-(octyloxy)phenyl) azo]phenoxy)pentane-1-thiol (TH2) containing azobenzene mesogenic group in the side-chain of the structure has

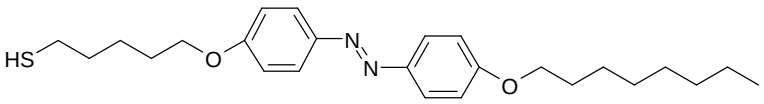

TH2

proceeded in four steps: Initial step was preparation of 4-(octyloxy)aniline by alkylation of 4-acetamidophenol and KOH mixture with octyl bromide. In the second step 4-hydroxy-4'-(octyloxy)azobenzene was synthesized by azocoupling of 4-(octyloxy)aniline with phenol. In the third step 4-[(5-bromopentyl)oxy]-4'-(octyloxy)azobenzene was prepared by the reaction of 4-hydroxy-4'-(octyloxy)azobenzene with 1,5-dibromopentane in dry acetone in the presence of K_2CO_3. Finally, thiuronium salt prepared from 4-[(5-bromopentyl)oxy]-4'-(octyloxy)azobenzene and thiourea was alkaline hydrolyzed yielding TH2. More details about TH2 synthesis can be found in [16]. TH2 was used in grafting reaction of the terminal thiol HS group with double bonds of PBD.

LCPBDs: In radical addition of TH2 onto double bonds of PBD 2,2'-azoisobutyronitrile (AIBN) was used as initiator. The reaction proceeded in toluene solution (54 g of PBD in 1 l of toluene) at the iniator-to-thiol ratio $5x10^{-2}$ mol at 60 °C for 48 h. We have synthesized SCLCPBDs with various initial molar ratios of thiols to double bonds of PBD, R_0, in the range from 0 to 1 (Table 4).

5.2.2 Characterization of SCLCPBDs: elemental analysis, NMR spectroscopy, GPC, WAXS and polarizing optical microscopy

The degree of modification, R_{eS} ([bound thiols]/[double bonds], mol/mol), after the addition and purification, was determined from elemental analysis using the relation

$$R_{eS} = 32 \times w_S / (54 + 427.6 \times w_S) \quad (43)$$

where w_S is the weight fraction of sulfur bonded in SCLCPBDs as determined by elemental analysis.

The degrees of modification were determined also by ^{1}H and ^{13}C NMR spectroscopy (300.1 MHz and 75 MHz, respectively, 60 °C). For R_{eNMR} determination the integrated intensity of the signal of OCH_2 of LC-thiol protons at 4.0 ppm (or the signal of aromatic protons) was used. In this case the detailed structure of SCLCPBDs (amount of 1,2 and 1,4 butadiene units [56], hydrogenated PBD units and OH end groups [57]) could be evaluated. Detailed structure of neat PBD and modified SCLCPBDs (amount of 1,2 and 1,4 butadiene units, hydrogenated PBD units and OH end groups) evaluated from ^{1}H NMR spectroscopic measurements is shown in Table 4.

The number- (M_n) and weight-average (M_w) molecular weights were determined by GPC (modular LC system with refractive index detection, column 30×8 SDV 10000) calibrated with PS standards. Tetrahydrofuran was used as solvent and measurements were carried out at room temperature. From M_n, values the degrees of modification, R_{eGPC} were determined.

Table 4*. ^{1}H NMR structure analysis of neat and modified SCLCPBDs*

R_0	R_{eNMR}.100	HPB mol.%	PB mol.%	pendant vinyl mol.%	trans+cis mol.%
0	-	5.1	94.9	61.5	33.4
0.2	21.8	24.1	54.1	25.3	28.8
0.4	39.3	23.5	37.2	12.8	24.4
0.6	54.0	17.5	28.5	7.7	20.8
0.8	74.0	4.5	21.5	4.5	17.0
1.0	83.9	0	16.1	1.6	14.5

Wide-angle X-ray diffractograms were taken on a HZG4A diffractometer (Freiberger Präzisionsmechanik, Germany) using Ni-filtered CuKα radiation. For high-temperature measurements a heating chamber with thermal stability of 0.5 °C was attached.

The texture of crystalline and LC phases was determined by a polarizing optical microscope (Nicon Eclipse 80i, crossed polarizer's equipped with a heating stage. The heating/cooling rate was 3 K/min.

5.2.3 Structure and degree of SCLCPBDs modification

It can be seen from Table 4 that with increasing initial molar ratio of thiol to double bonds of PBD, R_0, the fraction of grafted PBD monomer units increases; in addition, some amount of hydrogenated units (HPB) in SCLCPBDs is formed. While for unmodified PBD (R_0 = 0) fraction of HPB is ~ 0.05, after modification, the highest obtained value of HPB ~ 0.24 was for R_0 = 0.2; further increase in R_0 leads to a decrease in HPB and for R_0 = 1.0 fraction of HPB is 0. It is interesting to note that at the highest modifications practically all pendant (1,2) double bonds were consumed while a substantial amount of backbone (1,4) double bonds remained. This suggests that the SH groups of thiol preferably reacts with pendant double bonds of PBD. This finding is in agreement with previous results obtained on model reaction of thiyl radical which attacks the double bond of alkene; it was found that the reactivities of thiol with 1- and 2-alkenes differ [68]. ^{1}H and ^{13}C NMR spectroscopy has also proved that the OH functionality of SCLCPBDs does not change with the extent of the addition reaction.

Comparison of various experimental degrees of modification, R_e, obtained from GPC, R_{eGPC}, (from number-average molecular weights M_n), sulfur content, R_{eS}, and ^{1}H NMR analysis, R_{eNMR} in dependence on initial ratio R_0 is shown in Fig. 22. As expected, modification degrees R_{eS}, determined by all three methods, increase with increasing initial ratio R_0. While for the lowest initial thiol ratios R_0 ($R_0 \leq 0.4$), $R_0 \sim R_{eS}$, for higher R_0, $R_{eS} < R_0$ were found. Lower R_{eS} values suggest that at the higher R_0 values steric hindrance probably prevents the addition reaction and thiol is subsequently removed from polymer during purification. We believe that also dimerization of thiols can take place in the presence of initiator by recombination of thiol radicals; the lowest R_{eGPC} values suggest that some of these dimmers remain in the modified PBD even after purification.

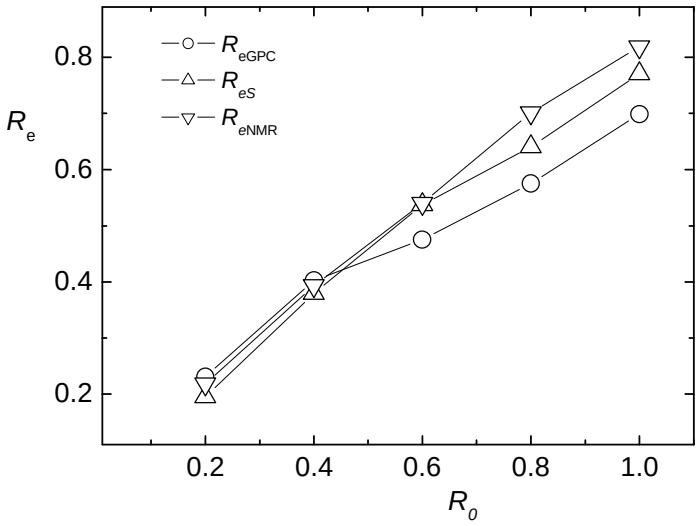

Fig. 22. *Determined degrees of modification R_e (from S content - R_{eS}, from GPC - R_{eGPC} and from ^{1}H NMR - R_{eNMR}) in dependence on on initial ratio of thiol/double bonds - R_0*

5.2.4 Thermal behavior

An example of measured DSC traces of neat thiol and SCLCPBD with R_0 = 1.0 is

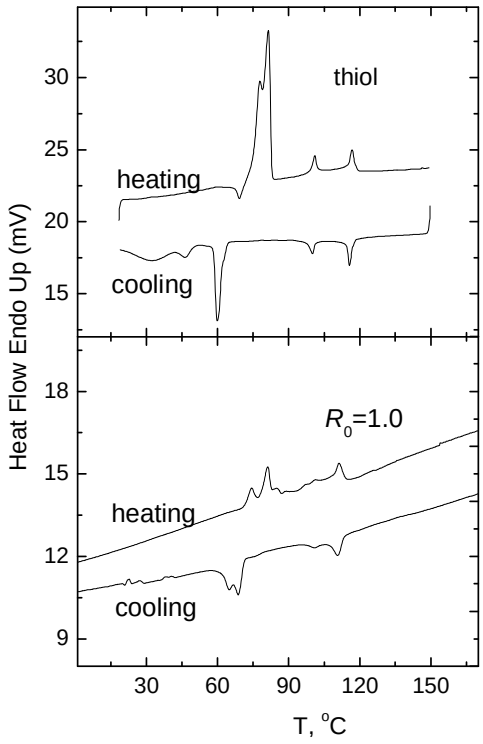

Fig. 23. *Example of measured DSC traces for neat thiol and SCLCPBDs with R_0 = 1.0. Cooling and heating rate was 10 K/min*

shown in Fig. 23; the corresponding transition temperatures (the glass transition - T_g and melting temperatures - T_m) determined from DSC thermograms in cooling (C) and subsequent heating (H) scans are summarized in Table 5.

***Table 5**. Degree of modifications and DSC transitions of thiol, PBD and SCLCPBDs*

R_0	R_{eS}	Run	T_g °C	ΔC_p J/g	T_{m1} °C	ΔH_{m1} J/g	T_{m2} °C	ΔH_{m2} J/g	T_{m3} °C	ΔH_{m3} J/g	T_{m4} °C	ΔH_{m4} J/g
thiol	0	H					81.4	60.8	100.9	2.7	116.9	3.2
		C			32.4	-18.3	59.9	-17.7	100.0	-2.6	115.6	-4.6
PBD	0	H	- 47.3	0.49								
		C	- 44.2	0.42								
0.2	0.195	H	-15.9	0.15	-8.3	1.3	54.8	5.2	89.5	0.8		
		C	-12.5	0.29			41.2	-3.1	80.2	-0.5		
0.4	0.379	H			-7.2	1.8	54.6	7.5	84.5	7.0		
		C			- 4.7	- 4.8			79.3	-3.3		
0.6	0.537	H					72.9	5.6			103.1	6.1
		C					60.2	-1.3			102.7	-9.7
0.8	0.641	H					73.1	11.8	85.6	3.8	105.1	8.9
		C					62.1	-8.7	74.7	-1.7	108.2	-9.5
1.0	0.771	H					74.7	3.7	81.2	11.4	111.3	7.1
		C					64.5	-5.9	74.5	-	110.9	-8.2

Wide-angle X-ray diffraction (WAXS) data for thiol and SCLCPBD with R_0 = 1.0 are shown in Fig. 24. From Table 5 it follows that on cooling of the thiol first mesophase formation takes place at ~ 116 °C (ΔH_m ~ - 4.6 J/g, SmA phase in which the centers of mass of the rods are in one dimensional periodic order parallel to long axes of the rods); next transition is at 100 °C (ΔH_m ~ - 2.6 J/g, SmC phase with tilted molecules to long axes); two smectic phases has been usually found in the case that azobenzene grouping is present in organic LC molecules with flexible spacer [69, 70]. WAXS measurements (Fig. 24) showed that at 95 and 77 °C diffractograms of thiol consist of one strong, narrow reflection the position of which corresponds to 3.04 nm and a broad amorphous halo. Theoretical atomistic simulations of thiol using software BIOSYM led to the length of ~ 3.2 nm, which agrees well with the found one. Due to this we assume that a smectic structures exist in thiol; this periodicity stays in crystalline phase at lower temperatures. The crystallization of TH2 on cooling takes place at ~ 60 °C (ΔH_m ~ -17.7 J/g). From WAXS measurements periodicities of 3.12 and 1.88 nm were determined at 70 °C; the amorphous profile is overlapped by several narrow reflections, which indicate a lateral order of thiol chains (especially of the mesogenic groups). As follows from Fig. 23 two transitions associated with reorganization of crystal phase have appeared at ~ 45 and 32 °C (sum of both ΔH_m ~ -18.3 J/g and denoted as T_{m1} in Table 5); periodicities of 4.9 and 2.52 nm were found at 60 °C from WAXS (Fig. 24). On subsequent heating, small recrystallization (Fig. 23) followed by melting of the crystalline phase at temperature ~ 81 °C (ΔH_m ~ 61 J/g) was observed (Table 5). At temperatures higher than 85 °C, a SmC structure appears; this structure melts at 101 °C (ΔH_m ~ 2.7 J/g) to SmA mesophase which finally melts to an isotropic state at 117 °C (ΔH_m ~ 3.2 J/g, Table 5).

From DSC traces of SCLCPBD with R_0 = 1.0 shown in Fig. 23 it follows that modification leads to simpler thermal behavior in comparison with neat thiol (see also Figs 24 and 25). On cooling only one mesophase seems to be formed at ~ 111 °C (ΔH_m ~ -8.2 J/g, Table 5); crystallization starts at ~ 75 °C (ΔH_m ~ -12.4 J/g) and final structure formation takes place at ~ 65 °C (ΔH_m ~ -5.9 J/g, Table 5). On heating crystalline structure melts at ~ 75 °C (ΔH_m ~ 3.7 J/g) and ~ 81 °C (ΔH_m ~ 11.4 J/g) to smectic mesophase which melts at ~ 111 °C (ΔH_m ~ 7 J/g). As expected, lower ΔH_m values were found for modified SCLCPBDs in comparison with those of neat thiol (Table 5). The T_g transition could be observed on DSC thermograms only for SCLCPBD with R_0 = 0.2; higher modifications exhibit only crystal/mesophase/isotropic state transitions (it is in agreement with dielectric results shown in Fig. 32). As T_g for SCLCPBD with R_0 = 0.2

has increased for about 30 °C we believe that for SCLCPBDs with R_0 > 0.2 the values of T_g have increased into temperature region of ordered phases formation.

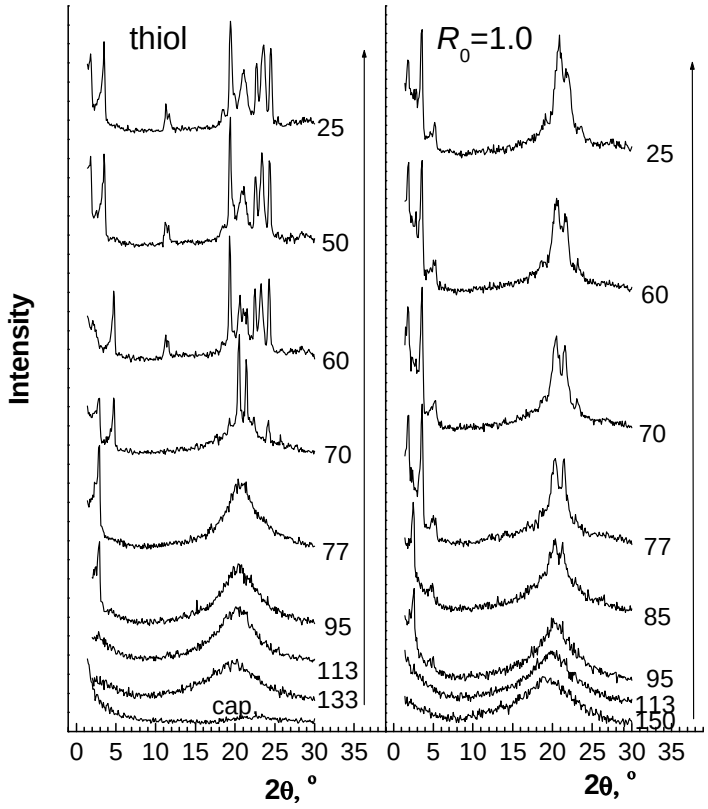

Fig. 24. *X-ray scattering diffractograms for thiol and SCLCPBD with R_0 = 1.0 obtained on cooling. The numbers at curves denote temperatures in ^oC*

From the WAXS patterns of SCLCPBD with R_0 = 1.0 (Fig. 24), it can be seen that on cooling the smectic structure in polymer is formed at 95 °C with the periodicities of ~ 3.39 and 1.7 nm (the first value agrees well with the length of the thiol molecule). At 85°C the crystallization starts and the amorphous profile is overlapped by reflections indicating lateral order of grafted chains. At 77 °C lamellar periodicities of 4.72, 2.45 and 1.7 nm, which reflect mutual ordering of grafted side-chains, were determined. Below 77 °C the same structure remains. On subsequent heating the diffractograms revealed a structure change from crystalline to LC smectic texture at 85 °C and at 95 °C; the same periodicities were determined as in the cooling regime (3.39 and 1.7 nm). Further heating above 115 °C melts the sample, and the diffractograms correspond to a completely amorphous structure of the polymer. Comparison of WAXS patterns of the thiol and SCLCPBD with R_0 = 1.0 reveals that even though in both samples similar ordered

structures were formed (Fig. 24) in thiol at the low temperatures better, a more extensive crystalline structure was developed. This is in agreement with Fig. 25 in which the temperature dependences of weight fractions of the ordered phase determined from X-ray diffractograms (from area below peaks) are shown. While almost all thiol is involved in

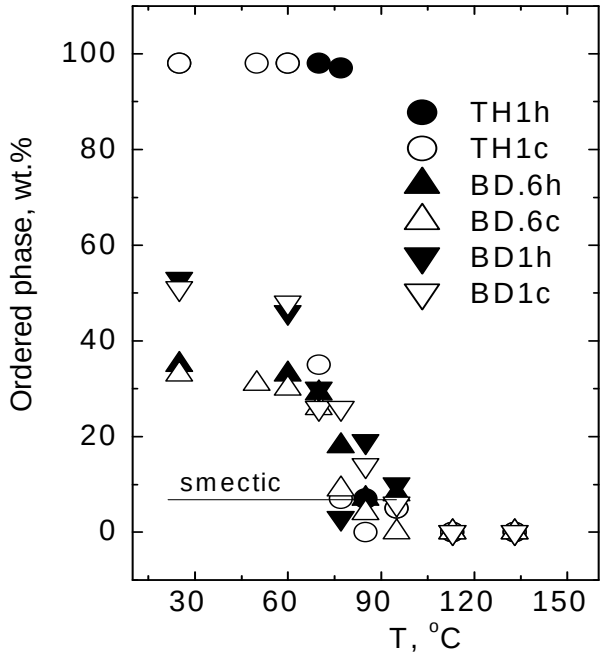

Fig. 25. *Temperature dependence of the weight fractions of the ordered phase determined on cooling (open symbols) and subsequent heating (full symbols) for thiol and SCLCPBD with R_0 = 0.6 (BD.6) and R_0 = 1.0 (BD1)*

the crystalline phase (98 – 95 wt.%) at the lowest temperatures, only ~ 33 wt.% and ~ 52 wt.% of sample is involved in the crystalline structure for SCLCPBDs with R_0 = 0.6 and 1.0, respectively. These results are also confirmed by polarizing microscopy measurements shown in Fig. 26; a better developed ordered smectic and crystalline structure can be seen for thiol than for sample with R_0 = 1.0.

As expected, simple amorphous behavior with only the glass transition temperature T_g was found for PBD; the change in the specific heat ΔC_p ~ 0.45 J/g.K shows a value typical of amorphous polymers [27] (Table 5). The same results for unmodified PBD of similar microstructure were obtained earlier by Hofmann et al. [71].

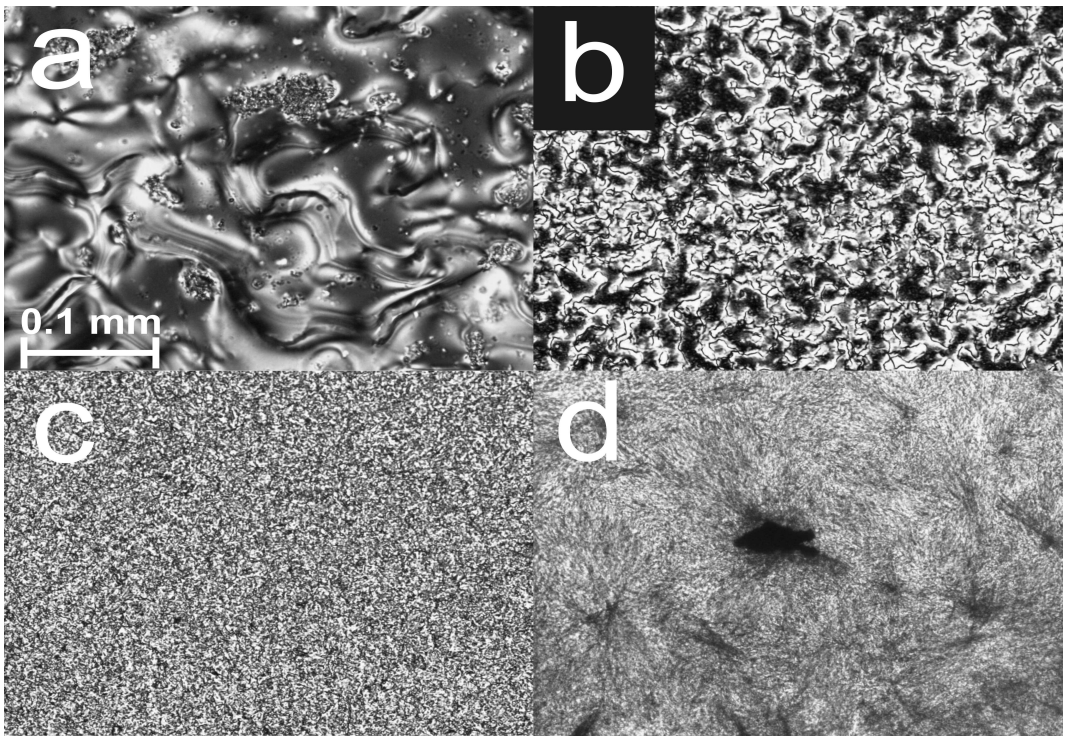

Fig. 26. *Optical micrographs of thiol (a,c) and SCLCPBD with R_0 = 1 (b,d): a - thiol 95 °C, b –LCPBD 95 °C; c - thiol 25 °C, d – SCLCPBD 25 °C*

5.2.5 Dielectric behavior

5.2.5.1 Temperature dependencies of dielectric behavior

Fig. 27 displays the temperature dependence of the real *ε´*(a), (a) and the imaginary *ε"* (b) component of the complex dielectric permittivity at a fixed frequency of 500Hz measured for the unmodified PBD and all the SCLCPBDs. Dielectric data were measured isothermally, upon heating from the solid state, as a function of frequency and represented as a function of temperature at a constant frequency; this plot allows to follow the overall dielectric behavior of the materials under study. In such representation contribution from each relaxation process is observed as a stepwise increase with increasing temperature, in the real part ***ε´*** and as a peak in the imaginary part ***ε"***. The change in molecular mobility, when passing from the crystalline state (where small

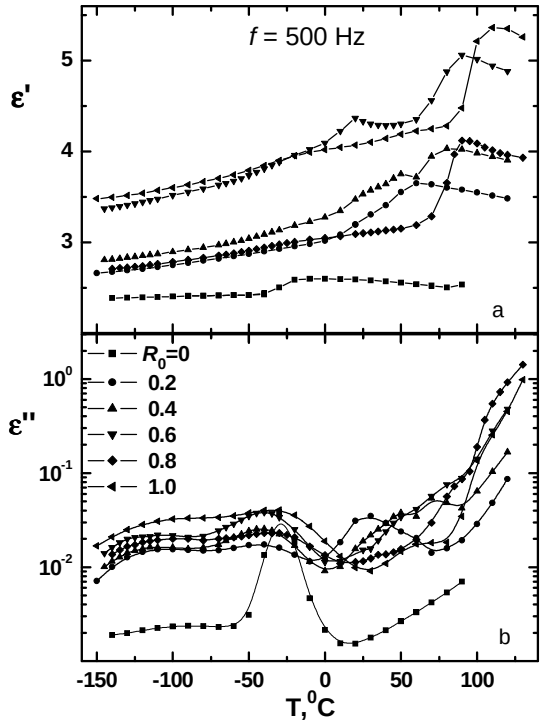

Fig. 27. *Temperature dependence of dielectric storage, ε´ (a), and dielectric loss, ε" (b) component measured at 500 Hz for unmodified PBD and SCLCPBDs*

scale motions can take place) to the intermediate liquid crystalline state (where collective motions may occur), can be followed as a significant increase in ε' with increasing temperature. Transition from the ordered to the isotropic liquid state is indicated by a decrease in ε' with increasing temperature as a result of the thermal motion which disturbs the orientation of molecular dipoles.

In unmodified PBD two processes are observed as peaks in ε" at ~ –30 ^{o}C and the small one at ~ -90 ^{o}C for the selected frequency (500Hz), can be observed (Fig. 27). The relaxations are assigned to the local motion of pendant vinyl groups (β-relaxation) and to the segmental motion of the main polymer chain (α-relaxation), respectively. The decrease in ε' at high temperatures (> 100 ^{o}C) is due to the thermal motion, which does not allow the orientation of the dipoles.

For SCLCPBDs, higher values of ε' are detected as compared with that of the unmodified PBD indicating a higher molecular mobility in the SCLCPBDs. This is due to incorporation of the thiol chains with polar groups into the PBD structure. The dependence of ε' on the R_0 is not linear, the polymers with high R_0 (0.6 and 1.0) are characterized by higher molecular mobility compared with those with lower R_0 (0.2 and 0.4). However, the maximum polarization increases nearly linear with the R_0 content

(with the exception of the sample with R_0 equal to 0.8) due to an increase in the amount of polar groups with increasing R_0.

At low temperatures, in the solid state, two processes take place in all of the SCLCPBDs observed as peaks in ε'' at ~ -40 and ~ -110 ^{o}C. We believe that these relaxations can be attributed, in the order of increasing temperature, to the local motion of the octyloxy end groups of the side-chain (γ-relaxation), and to the motion of the azobenzene moiety of the side-chain around its long molecular axis (β-relaxation) without involving the motion of the side-chains as a whole.

A significant change in ε' is observed (for the selected frequency) at temperatures above 0 ^{o}C for the SCLCPBDs with R_0 equal to 0.2 and 0.4. For the SCLCPBDs with R_0 equal to 0.6, 0.8 and 1.0, this change is observed at temperatures above 50 ^{o}C. This change indicates a significant change in the molecular mobility of the polymers above the temperatures mentioned above, which correlates with the melting temperatures found by DSC measurements (Table 5).

A further increase in the temperature (above 90 ^{o}C) results in a decrease in ε' as a result of molecular thermal motion, which does not allow the orientation of the dipoles; the finding indicates the transition of the materials to the isotropic state. This means that at temperatures higher than the temperature at which the temperature coefficient of ε' changes from positive to negative, the materials are in the liquid state. The temperature at which transition to the isotropic state occurs increases with increasing R_0 and is in good agreement with the clearing temperatures found by polarizing microscopy and DSC measurements (Table 5). In the liquid crystalline state, the picture of the relaxation processes is complex, consisting of one or two peaks while in the isotropic state only dc conductivity maintains (a steep increase in ε'' with increasing temperature).

5.2.5.2 Frequency dependencies of dielectric behavior

Fig. 28 displays the frequency dependences of the imaginary part of the dielectric permittivity, ε'', for the unmodified PBD in the temperature range between –35 and 5 ^{o}C. A well-resolved peak, which shifts to higher frequencies with increasing temperature, can be observed. This peak corresponds to the main relaxation (α), which is associated with the cooperative motion of segments of PBD backbone chains and is related to its glass transition.

As an example of the measured frequency dependences of the dielectric losses in the SCLCPBDs, data for the material with R_0 equal to 0.2 at several temperatures in the

crystalline (a) and liquid crystalline (b) state are presented in Fig. 29. Two dielectric dispersions are observed

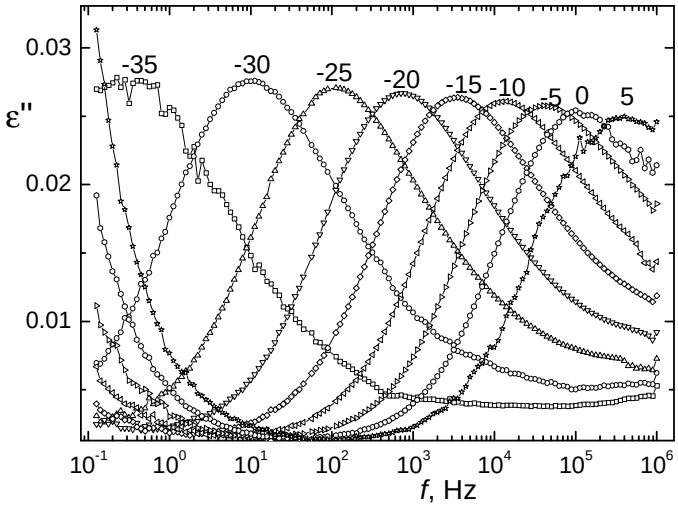

Fig. 28. *Frequency dependence of dielectric loss, ε″, for PBD in the region of the main α-relaxation. The numbers at curves denote temperatures in ^oC*

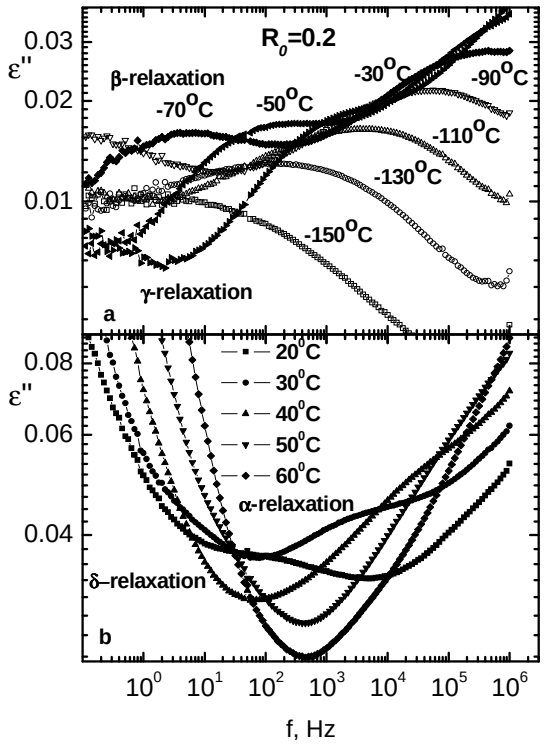

Fig. 29. *Dielectric loss component ε″ as a function of frequency for the SCLCPBD with R_0 = 0.2 at low (γ and β relaxation (a)) and high (α and δ relaxations (b)) temperatures*

in the crystalline state at the lowest frequencies (Fig. 29a). The γ-relaxation is observed at very low temperatures as a broad peak which shifts to higher frequencies with increasing temperature. The γ relaxation peak is followed by a narrower β relaxation peak detectable in the frequency window of dielectric measurements in the temperature range between –50 and 0 ^{o}C. The same relaxations are observed for all the SCLCPBDs, a detailed analysis and discussion of them follows. The assignment of these relaxations to particular molecular motions has been done in the previous subsection.

At high temperatures two dispersions are also observed (Fig. 29b). The faster relaxation, observed as a shoulder on ε'' vs. f dependences, shifts from 100 Hz at 20 ^{o}C to 100 kHz at 60 ^{o}C, while the slower relaxation is observed as a change in the slope of ε'' vs. f at low frequencies. The faster relaxation is attributed to α-relaxation, which is associated in liquid crystalline polymers with reorientations of the polymer backbone and spacer, while the slower relaxation is attributed to the δ-relaxation. The α relaxation is observed only for the polymer with R_0 = 0.2, while the δ-relaxation is observed as a well-resolved peak for the materials with R_0 = 0.4, 0.6 and 0.8. The increase in ε'' with decreasing frequency observed at low frequencies in Fig. 29b originates from the propagation of mobile charge carriers (conductivity contribution) [53].

In order to extract quantitative information on the time scale, as well as on the strength and shape of the observed dielectric relaxations, the decomposition procedure for fitting the data was used. In principle, the HN function (eq. (28)) is used for the description of frequency dependences of an individual relaxation process. This method works well when all processes are reasonably separated, as in the case of the α-relaxation in the PBD. When they start to overlap (as in the case of relaxation processes in SCLCPBDs), the fitting procedure is getting difficult (e.g., HN parameters, which determine the high frequency part of the β-relaxation, and those which characterize the low-frequency part of the γ-relaxation affect each other [53]). Because of the problem mentioned above we assumed that all relaxations observed in the SCLCPBDs are well described by the simpler Cole-Cole distribution function, which results from the HN function with the b parameter equal to 1. The fitting procedure was based mainly on the frequency dependences of the imaginary part of dielectric permittivity ε''.

An example of the fitting procedure is presented in Fig. 30 for the material with R_0 = 0.6 for the γ-, β- and δ-relaxations in the order of increasing temperature. The sharp increase in dielectric losses with decreasing frequency observed at the highest

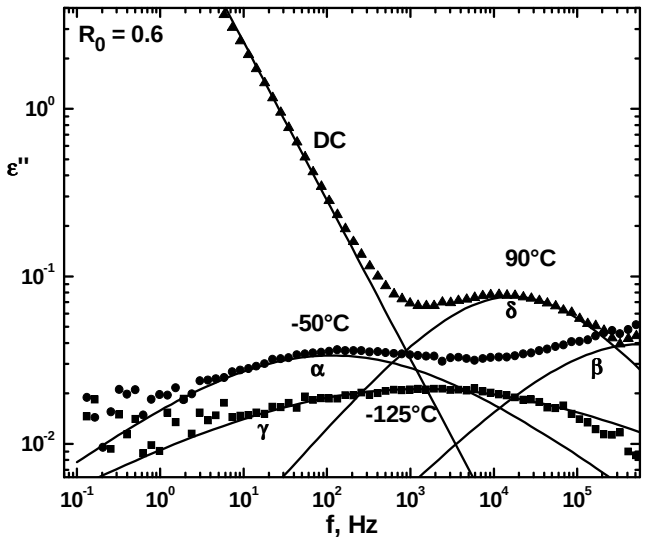

***Fig. 30**. An example of decomposition of ε″ vs. f dependences measured at indicated temperature for SCLCPBD with R_0 = 0.6*

temperatures corresponds to the conductivity contribution and was fitted by adding the term given in eq. (28) to the Cole-Cole function used for the δ relaxation. Two dielectric dispersion regions (γ and β) could be determined from the data measured at –50 ^{o}C, while for the lowest presented temperature (-125 ^{o}C) only a single process (γ relaxation) is observed. In some the cases information was extracted from the temperature dependence of ***ε"*** at a fixed frequency (isochronal plot). The results of the above analysis for each relaxation observed in the PBD and the SCLCPBDs, can be summarized as follows:

a) Unmodified PBD

a1) *α-relaxation*

The α-relaxation peak is well described by the HN equation with mean values (with respect to temperature) of the shape parameters *a* and *b* equal to 0.7 and 0.4, respectively, indicating a relatively narrow and unsymmetrical peak with a slope on the low-frequency side higher than that on the side of high frequencies. The relaxation strength $\Delta\varepsilon.T$ was found to be nearly temperature-independent (a mean value of $\Delta\varepsilon$ is equal to 0.14 at room temperature), which is reasonable because of the nonpolar character of polybutadiene. The temperature dependence of the peak frequency f_m of the α-relaxation is well described by the VFT equation with parameters $f_\infty = 10^{11}$ Hz, B = 1409 K and T_{VFT} = 127 K (Fig. 31, full squares).

The glass transition temperature obtained from the dielectric data as the temperature at which the relaxation time is equal to 100 s [53], known as $T_{g,diel}$ is equal to -42 ^{o}C (obtained by extrapolation of the VFT fitting curve to low frequencies) correlates well with the glass transition temperature measured by calorimetric measurements (Table 5). The glass transition temperature is in agreement with that reported in literature for polybutadiene with the same fraction of pendant-vinyl and linear butadiene units [72].

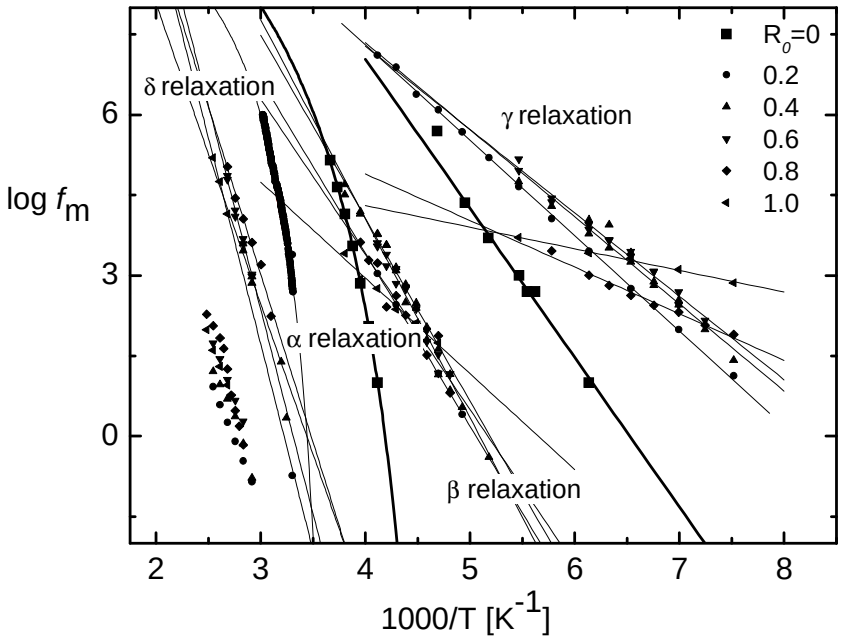

Fig. 31. *Logarithm of the peak frequencies f_m as a function of inverse temperature for all the observed relaxations in PBD and SCLCPBDs (Arrhenius diagram). The lines are fittings of the dielectric data to the VFT or Arrhenius equation (depending on the relaxation process)*

a2) γ-*relaxation*

γ-relaxation of neat PBD can be followed only in the isochronal plot. The temperature dependence of the γ-relaxation time, shown in Fig. 31 (full squares), follows the Arrhenius behavior, which is consistent with the origin of the relaxation i.e. movement of 1,2 and 1,4 groups of butadiene units. The values of activation energy E_a (0.43eV) and pre-exponential frequency factor f_∞ (10^{15} Hz), calculated by linear fit to the data of the logarithm of peak frequency f_m vs. $1/T$ (Arrhenius eq. (37)), indicates a local process.

b) SCLCPBDs

b1) *γ-relaxation*

The strength of the γ-relaxation was found to increase slightly with increasing temperature, with the shape parameter *a* between 0.17 and 0.20, for all the materials without any specific dependence on composition. This relaxation, associated with movement of aliphatic end of side-chains, becomes narrower as the temperature increases as it is expected for local relaxations; this reflects the homogenization of the environment of relaxing unit with increasing temperature. The mean value of the *b* parameter of the HN equation varies between 0.25 and 0.30 indicating a very broad relaxation. In the γ-relaxation peak of SCLCPBDs also the γ-relaxation of PBD can contribute due to a similar relaxation time of the two processes. However, the contribution of the γ-relaxation of PBD is expected to be less pronounced with increasing R_0 value, due to a decrease in the vinyl group content (Table 4).

The temperature dependence of the peak frequency f_m of the γ-relaxation of all SCLCPBDs can be described by the Arrhenius equation (eq. (37), Fig. 31). The parameters of the Arrhenius equation (activation energy E_a and pre-exponential factor f_∞) are listed in Table 6.

Table 6*. Parameters of Arrhenius equation for the dielectric relaxations of SCLCPBDs*

[thiol]/[PBD]	γ relaxation		β relaxation		δ relaxation	
R_0 mol/mol	f_∞ Hz	E_a eV	f_∞ Hz	E_a eV	f_∞ Hz	E_a eV
0.2	$3x10^{14}$	0.35	$2x10^{16}$	0.64	-	-
0.4	$6x10^{13}$	0.32	$5x10^{17}$	0.68	$1x10^{19}$	1.1
0.6	$3x10^{13}$	0.31	$1x10^{19}$	0.74	$1x10^{25}$	1.5
0.8	$2x10^{8}$	0.17	$1x10^{15}$	0.57	$1x10^{22}$	1.2
1.0	$1x10^{6}$	0.08	$1x10^{10}$	0.35	$1x10^{25}$	1.5

The values of E_a and f_∞ indicate a locally activated process. Extraordinary low values for both parameters are calculated for the materials with high contents of side-chains (R_0 = 0.8 and 1.0).

b2) *β-relaxation*

The strength $\Delta\varepsilon T$ of the β-relaxation does not depend on temperature while it increases with increasing R_0, with the exception of the polymer with R_0 = 0.8, which in general is characterized by very low values of dielectric permittivity indicating a material with suppressed molecular mobility. The strength $\Delta\varepsilon$ ranges from 0.1, for the material with R_0 = 0.2 to 0.3 for the sample with R_0 = 1.0. This result is consistent with the interpretation given for this relaxation: with increasing R_0 the content of polar groups, which contribute to the β-relaxation, increases. The shape of the relaxation remains unchanged with temperature and it is almost independent of composition, while the value of α-parameter of HN was found equal to 0.4 for all samples.

The temperature dependence of the peak frequency is well described by the Arrhenius equation (eq. (37), Fig. 31). For both activation parameters (E_a, f_∞) extraordinary high values are obtained (Table 6). Similar high values of E_a and f_∞ have been reported in literature for side-chain liquid-crystalline polymers with the polar azobenzene moieties in side-chains [53]. It was argued that this relaxation is associated not only with local motion of the mesogen in the potential formed by the surrounding molecules. Instead, it was suggested that neighboring molecules are involved as well in the liberation dynamics of the β-relaxation. The values of E_a and f_∞ were found to increase with increasing R_0, except for the materials with R_0 = 0.8 and 1.0.

b3) *α-relaxation*

The α-relaxation was observed only for the composition with the lowest R_0 = 0.2; this finding corresponds to DSC data (Table 5). The relaxation is observed as a peak in isothermal measurements of dielectric losses only at three temperatures in the frequency window of dielectric measurements. On the other hand, it can be followed in isochronal plots of dielectric losses as a peak which shifts to higher temperatures with increasing frequency. Because of the limited data for this relaxation from the isothermal data (the fitting was possible only for three temperatures), the information was extracted from the isochronal plots. The α-relaxation in the SCLCPBD with R_0 = 0.2 is observed at higher temperatures or lower frequencies as compared with that observed in unmodified PBD, indicating an increase in the glass transition temperature T_g in SCLCPBDs. The maximum of the dielectric losses increases only insignificantly, which is unexpected as in this type of relaxation, motion of segments with higher dipole moments is involved. The results can be understood in terms of an increase in stiffness of the main-chain due to the

interaction of pendant vinyl butadiene units with the SC units (strongly interacting), as was found by ^{1}H NMR measurements, resulting in a reduced segmental mobility.

At high temperatures the relaxation rate follows the Arrhenius behavior with extraordinary high values of activation energy and pre-exponential frequency factor (2.0 eV and 10^{38} Hz), which turns to a VFT-like dependence, indicating a change in the molecular dynamics of the system (Fig. 31). Fitting of the data to the VFT equation gives for the parameters of the equation, f_∞, B and T_{VFT}, the values 10^{11} Hz, 808 K and 258 K, respectively. The temperature at which the change of molecular dynamics occurs agrees with a phase transition temperature of the system - melting of crystalline phase as detected by DSC measurements. Finally, the maximum of dielectric losses as recorded from the isochronal plots was found to increase with increasing temperature. It can be assumed that this relaxation is suppressed in materials with higher R_0 as a result of the higher content of the ordered phase in samples.

b4) *δ-relaxation*

Information about the δ relaxation is limited for some polymers; it can be extracted for few temperatures. The fitting procedure for the δ-relaxation was possible only for the materials with R_0 = 0.4, 0.6 and 0.8. From the limited data for the shape parameter, a, and the intensity, $\Delta\varepsilon$, of the δ-relaxation, it can be concluded that the relaxation is narrow with an a parameter which ranges from 0.5 for the sample with R_0 = 0.4 to 0.7 for that with R_0 = 0.8. The strength of the relaxation $\Delta\varepsilon$ is approximately 0.2 and 0.5 for the materials with R_0 = 0.4 and 0.6, respectively at the temperature of relaxation. For the sample with R_0 = 0.8, a lower value of $\Delta\varepsilon$ was found. The maximum of dielectric losses decreases with increasing temperature in the smectic phase and levels off in the isotropic state. The limited temperature data for this relaxation does not allow to conclude on the temperature dependence of its peak frequency f_m (Arrhenius or VFT behavior) (Fig. 31). Assuming the Arrhenius behavior, extraordinarily high values were calculated for the E_a and f_∞ (Table 6), indicating a cooperative process. The cooperative character of this relaxation has been discussed in the literature [73]. In the smectic A phase this processes is interpreted as being due to the side group flipping around the polymer backbone as the mesogen is hopping from one smectic layer to another [74]. This interpretation agrees well with the fact that in isotropic phase no such relaxation is observed, while the absence of this process in the material with R_0 = 0.2 may reflect the lower order within this sample as a result of the low side group content.

b5) *DC conductivity*

The information about the DC conductivity observed at high temperatures was extracted from analyses of the imaginary part of the complex electric modulus *M"* in dependence on frequency (eq. (41), Fig. 32). Representation of the data using the electric

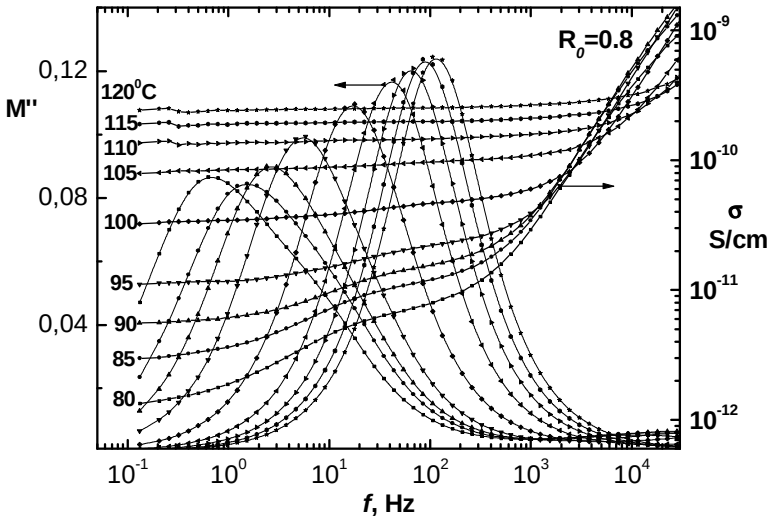

Fig. 32. *Frequency dependence of the imaginary part of the complex electric modulus, M" (left axis) and of the real part of complex conductivity, σ (right axis), for the SCLCPBD with R_0 = 0.8 at high temperatures, indicated on the plot*

modulus formalism allows the observation of the conductivity as a peak on its frequency dependence, which is more convenient for analysis. As an example of the dependences of conductivity σ and electric modulus *M"* as a function of frequency in a high temperature range related with conductivity phenomena for the material with R_0 = 0.8 is demonstrated in Fig. 32. A significant increase in conductivity is observed in the temperature range 95-105 ^{o}C, as compared with the increase in conductivity with temperature at temperatures below 95 ^{o}C and above 105 ^{o}C; this indicates a change of the charge carrier mobility. The temperatures are in good agreement with the transition temperatures obtained by DSC measurements on these samples (Table 5). In the frequency dependence of the imaginary part of *M"*, a peak at 80-90 ^{o}C with a double structure can be observed, which narrows with no indication of double structure at higher temperatures. The relaxation observed as a shoulder at the high frequency region corresponds to relaxation with interfacial character i.e. corresponds to the Maxwell-Wagner-Sillars (MWS) type polarization as a result of the existence of layers with different conductivity within the material; peak observed at low frequencies corresponds to the conductivity relaxation due to the

transport of mobile charge carriers. MWS polarization is observed also in the materials with R_0 = 0.6 and 0.8, indicating electrically heterogeneous materials due to the formation of the ordered smectic phase.

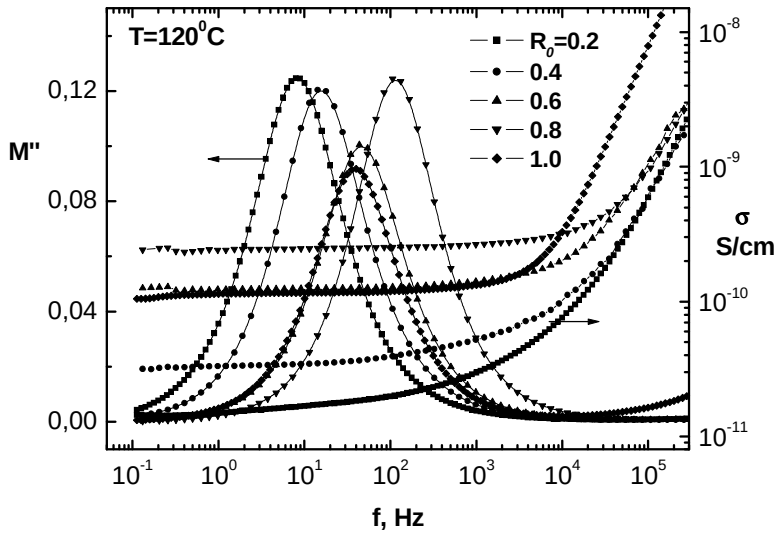

Fig. 33. *Frequency dependence of the imaginary part of the complex electric modulus, M"(left axis) and of the real part of complex conductivity, σ (right axis), for all the SCLCPBDs at 120 ^{0}C (isotropic state)*

Figure 33 displays the frequency dependences of *M"* and σ for all the materials at 120 ^{o}C (isotropic state). The materials can be classified into two groups; materials with R_0 = 0.2 and 0.4 and materials with R_0 = 0.6, 0.8 and 1.0, which differ in conductivity values by an order of magnitude and in peak frequency by one decade (peak shifts to higher frequencies with increasing conductivity).

The temperature dependence of the main peak frequency f_m (determined from the *M"* vs. *f* dependences) can be described by the Arrhenius equation (eq. (37), Fig. 34). For the materials with R_0 = 0.4 and 0.8, significant changes in the relaxation rate, passing from the smectic to the isotropic state is observed; this indicates a change of the mobility of the charge carriers in the two phases. For the material with R_0 = 0.4, the Arrhenius equation with E_a = 1.55 eV and 0.79 eV and $f_\infty = 10^{22}$ Hz and 10^{11} Hz fits well to the data in the smectic and the isotropic phase, respectively. The corresponding values for the material with R_0 equal to 0.8 were found to be equal to 1.58 eV and 0.75 eV, and 3.10^{22} and 10^{12} Hz, respectively.

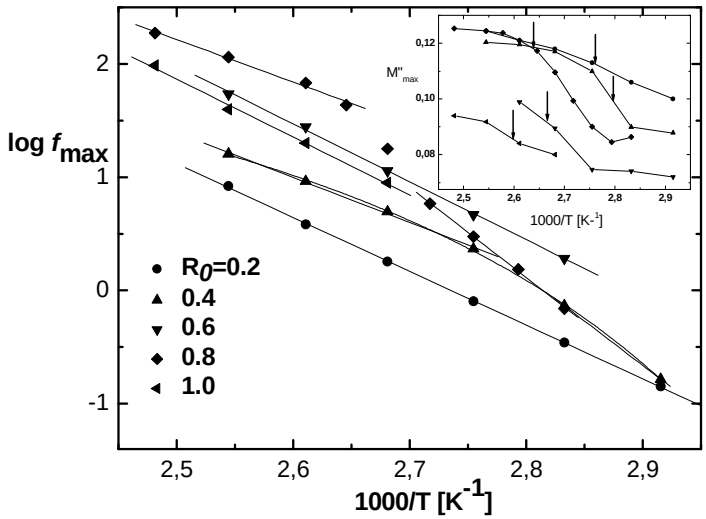

Fig. 34. *Logarithm of the M" peak frequency f_m, related to the conductivity, versus inverse temperature (Arrhenius diagram). Inset shows the dependence of the magnitude of the maximum of electric modulus, M"$_{max}$, on the inverse temperature (arrows indicate the clearing temperatures found by DSC measurements)*

The higher activation energies calculated for the smectic phase reflect the difficulty of the charge carriers to move within this phase. For the materials with R_0 = 0.2, 0.6 and 1.0, the Arrhenius equation was fitted in the whole temperature range with parameters 0.94 eV, 1.0 eV and 1.0 eV, and 10^{13} Hz, 10^{15} Hz and 10^{15} Hz, respectively.

A significant change of the magnitude of the *M"* maximum was observed at the clearing temperature for all the materials as can be followed in the inset of Fig. 34, where the clearing temperatures, corresponding to the highest T_{mi} (DSC measurements), are indicated by arrows. *M"$_{max}$* increases significantly with temperature increasing to the clearing temperature and becomes almost constant in the isotropic phase. This behavior can be understood in terms of an increase in the charge carrier concentration, which contributes to conductivity, due to the increase in molecular mobility passing from the smectic to the isotropic state.

Finally we should mention that SCLCPBD with R_0 = 0.4 was used also for optical investigations at room temperature [16]. It was found that: (1) photochemically induced trans-cis-trans isomerization of azobenzene groupings results in their local reorientation upon irradiation with linearly polarized UV light. (2) resulting dichroism and birefringence are stable and can be erased by subsequent irradiation with non-polarized light. Further irradiation with polarized light induces anisotropy again. Points (1) and (2)

suggests that SCLCPBDs and also linear and crosslinked materials based on these SCLCPBDs can be used for reversible optical data storage in photonics.

6. Conclusions

We have investigated the relations between structure, thermal and physical properties of SCLCPBDs with the comb-like architecture which were synthesized from PBD and two thiols with different structure of mesogenic group (cyanobiphenyl and/or azobenzene); polymers with various degree of modification of PBD chain were studied. From our investigation the following conclusions could be made:

(1) In the case of SCLCPBDs with cyanobiphenyl mesogenic group it was found:

(a) On GPC chromatograms two peaks gradually appear with increasing modification degree; this fact is probably associated with different rate constants of the addition reaction of thiol's SH groups on pending (1,2) and main-chain (1,4) double bonds of PBD. It was found that only ~50 % modification of PBD can be achieved even for stoichiometric initial ratio of SH/double bonds. NMR spectroscopy has proved that the functionality (OH group content) of SCLCPBDs does not change with the extent of modification.

(b) Simple amorphous behavior with the glass transition only was found for neat PBD and polymer with the smallest degree of modification R_{eS} = 0.13 (R_{eS} was determined from sulfur elemental analysis). With increasing R_{eS}, the T_g of SCLCPBDs increases from -46 °C (neat PBD) to 20 °C (R_{eS} ~ 0.51); at the same time the changes in the specific heat, ΔC_p, decrease. LC mesophase formation starts at R_{eS} ~ 0.27 (T_m ~ 27 °C); with increasing R_{eS} the melting temperatures T_m increase and for R_{eS} ~ 0.51 reach the value ~ 74 °C (corresponds to T_m of neat thiol).

(c) Large changes in the position and shape of the superimposed dynamic mechanical functions on the reduced frequency were found. While at the lowest frequencies the Newtonian liquid behavior was observed for neat PBD, for modified polymers more complicated frequency dependences were observed. In particular, SCLCPBD with the highest degree of modification (R_{eS} = 0.51), due to strong physical interactions of side-chain mesogens (which act as physical crosslinks), exhibits almost critical gel mechanical behavior at the gel point.

(d) The investigation of SCLCPBDs using broadband dielectric spectroscopy was also done. Four relaxation processes have been identified: γ, β, α and δ, in the order of

increasing temperature or decreasing frequency. The γ process is related to motion of 1,2 and 1,4 groups of butadiene units, the β- relaxation corresponds to liberation fluctuations of mesogens around their long molecular axis and the α-relaxation is assigned to fluctuations of segments of the polymer main-chain as they are observed in glass-forming systems. The δ-relaxation is assigned to liberation fluctuations of mesogens around the short molecular axis; presumably it is a rather multistep process with motional averaging rather than a 180 flip-flop jump of the mesogens [15, 60]. All dielectric relaxation processes were analyzed and discussed in terms of time scale (Arrhenius diagram), magnitude (relaxation strength) and shape of the response.

(2) In the case of SCLCPBDs with azobenzene mesogenic group it was found:

(a) As in previous case experimental modifications determined from sulfur elemental analysis, ^{1}H NMR spectroscopy and GPC, comb-like SCLCPBDs are always lower than initial SH/double bonds ratio; it was found that ca. ~ 70 % modification of PBD can be achieved. NMR spectroscopy has proved that the OH functionality of SCLCPBDs does not change in the modification.

(b) From the DSC and WAXS experiments it could be concluded that on cooling a smectic structure in the polymers is formed at 95 °C with the periodicity ~ 3.39 and 1.7 nm (the former value agrees well with the length of the thiol molecule). At 85 °C the crystallization starts and at 77 °C lamellar periodicities of 4.72, 2.45 and 1.7 nm, reflecting mutual ordering of grafted side-chains, are formed. The amount of ordered phase in the polymers increases with increasing modification.

(c) A simple dielectric behavior with segmental α-relaxation and secondary γ-relaxation was found for unmodified PBD. Two low temperature γ- and β-relaxations were observed for SCLCPBDs and assigned to the local motion of the octyloxy end groups (γ) of the side-chains, and to the motion of the azobenzene moiety of the side-chain around its long molecular axis. At higher temperatures, α-relaxation was observed only for neat PBD and SCLCPBD with the lowest R_0 = 0.2; for modified polymers α-relaxation is shifted to higher temperatures or lower frequencies with respect to neat PBD. We assume that α-relaxation is suppressed in the SCLCPBDs with higher R_0 due to a higher order in the smectic phase, formed within them. The δ-relaxation, assigned to liberation fluctuations of mesogens around the short molecular axis, was observed at temperatures higher than those of the α-relaxation in the SCLCPBDs with R_0 = 0.4, 0.6 and 0.8. As in previous

case dielectric relaxations were analyzed and discussed in terms of time scale (Arrhenius diagram), magnitude (relaxation strength) and shape of the response.

(d) Conductivity and interfacial Maxwell–Wagner–Sillars relaxation, indicating electrically heterogeneous materials due to the formation of the ordered smectic phase, were investigated by analyzing the data within the conductivity and the electric modulus formalisms. Dielectric behavior (in particular $\varepsilon'(T)$ at constant frequency), individual relaxations (α and δ) and conductivity exhibit distinct changes at the phase transition temperatures determined by DSC.

7. References

1. M. Gordon, N. A. Plate (Eds.), “Liquid Crystal Polymer II/III”, Adv. Polym. Sci, 60/61, 176-189, 1984
2. V. P. Shibaev, L. Lam, “Liquid Crystalline and Mesomorphic Polymers”, Springer-Verlag, Berlin, 1994
3. W. Meier, H. Finkelmann, Makromol Chem Rapid Commun; 11:1253, 1990
4. P. Bladon, M. Warner, Macromolecules; 26:1078, 1993
5. A. Bobrovsky, N. Boiko, V. Shibaev, J. Stumpe, Photochem Photobiol A; 163:347, 2004
6. E. Schab-Balcerak, B. Sapich, J. Stumpe, Polymer; 46:49, 2005
7. T. Tang, F. Zeng, S. Wu, Z. Tong, D. Luo, W. She, Opt Mater ; 27:585, 2004
8. Y. K. Han, B. S. Ko, Opt Mater; 21:621, 2002
9. M. Dumont, E. Osman, Chem Phys; 245:437, 1999
10. S. Jin, M. Wübbenhorst, J. van Turnhout, W. Mijs, Macromol Chem Phys; 197:4135, 1996
11. M. Wübbenhorst, E. van Koten, J. Jansen, W. Mijs, J. van Turnhout, Macromol Rapid Commun; 18:139, 1997
12. N. G. McCrum, B. E. Read, G. Williams, “Anelastic and Dielectric Effects in Polymeric Solid”, Dover Publications, New York, 1991
13. A. Jigounov, Z. Sedláková, J. Spěváček, M. Ilavský, Eur. Polymer J; 42:2450, 2006
14. R. Zentel, G. Strobl, H. Ringsdorf, Macromolecules, 18:960, 1985
15. F. Kremer, A. Schoenhals, Eds., “Broadband Dielectric Spectroscopy”, Springer-Verlag, Berlin, 2003
16. D. Rais, Y. Zakrevskyy, J. Stumpe, S. Nešpurek, Z. Sedláková, Opt Mater, submitted
17. B. Hahn, V. Percec, Macromolecules, 20:2961, 1987
18. V. P. Shibaev, N. A. Plate, “Thermotropic Liquid Crystalline Polymers with Mesogenic Side Groups”, Adv. Polym. Sci., 60/61, 179-201, 1984
19. G. Vertogen, W. H. de Jeu, “Thermotropic Liquid Crystals, Fundamentals“, Springer- Verlag, Berlin, 1988
20. H. Finkelmann, G. Rehage, “Liquid Crystal Side Chain Polymers”, Adv.Polym.Sci., 60/61, 99-172, Springer- Verlag, Berlin, 1984

21. C. B. McArdle, “Side Chain Liquid Crystal Polymers”, Blackie, Glasgow, 1989
22. B. Reck, H. Ringsdorf, Makromol. Chem. Rapid Commun. 6, 291 1985
23. B. Reck, H. Ringsdorf, Makromol. Chem. Rapid Commun. 7, 389 1986
24. J. Watanabe, M. Goto, T. Nagase, Macromolecules 20, 298 1987
25. A. Blumstein, “Liquid Crystalline Order in Polymers”, Academic Press, New York, 1978
26. L. Chapoy, “Recent Advances in Liquid Crystalline Polymers”, Applied Science, Elsevier, London, 1985
27. J. D. Ferry, “Viscoelastic Properties of Polymers”, 3rd ed., Wiley, New York, 1980
28. S. Jin, “Synthesis and Characterization of Side-Chain Liquid Crystalline Polyesters and Ploy urethanes”, 1997
29. S. Onogi, T. Asada, “Rheology and Rheo-optics of Polymer Liquid Crystals, Proceedings of the Eight International Congress on Rheology”, 1:127, Plenum Press, New York, 1980
30. M. Mours, H. H. Winter, “Experimental Methods in Polymer Science: Modern Methods in Polymer Research and Technology”, Academic Press, San Diego CA., 2000
31. C. Kittel, “Introduction to Solid State Physics”, John Wiley & Sons, 1976
32. P. Debye, “Polar Molecules”, Dover, New York, 1945
33. B. Sedlak, R. Bakule, “Elektrina a Magnetismus”, SPN, Praha, 1980
34. J. S. Toll, Physical Review, 104:1760, 1956
35. C. J. F. Bottcher, P. Bordewijk, “Theory of Electric Polarization”, vol II, Elsevier, New York, 1978
36. S. Havriliak Jr., S.J. Havriliak, “Dielectric and Mechanical Relaxation in Materials”, Carl Hansen Verlag, New York, 1997
37. N. G. McCrum, B. E. Read, G. Williams, “Anelastic and Dielectric Effects in Polymer Solids”, Wiley, London, 1967
38. P. Hedvig, “Dielectric Spectroscopy of Polymers”, Academiai Kiado, Budapest, 1977
39. M. E. Bauer, W. H. Stockmayer J.Chem.Phys., 43:4319, 1965
40. W. H. Stockmayer, Pure Appl. Chem., 15:539, 1967
41. J. K. Moscicki, A. A. Coller (Eds.), “Liquid Crystal Polymers – from Structure to Applications”, Elsevier, New York, 1992

42. F. Kremer, S. U. Vallerien, R. Zentel, H. Kapitza, Macromolecules, 22:4040, 1989
43. S. U. Vallerien, F. Kremer, C. Boeffel, Liq Cryst 4:9, 1989
44. A. Schonhals, D. Wolf, S. Weidner, Springer J, ACS polym Prepr 40:502, 1999
45. A. Schonhals, U. Gesner, J. Rubner, J Macromol Chem Phys 196:1671, 1995
46. R. Zorn, G. B. McKenna, L. Willner, D. Richter, Macromolecules, 28:8552, 1995
47. S. Esselin, L. Bosio, C. Noel, G. Decobert, J.C. Dubois, Liquid Crystals, 2:505, 1987
48. B. Wunderlich, J. Grebowicz, Adv. Polym. Sci., 60/61, 1, 1988
49. H. Stevens, G. Rehade, H. Finkelmann, Macromolecules, 17:851, 1984
50. V. P. Shibaev, N. A. Plate, Pure Appl. Chem. 57:1589, 1985
51. J. Doucet, G.R. Luckhurst and G.W. Gray (Eds.), "Molecular Physics of Liquid Crystals", Chapter 14, Academic Press, New York, 1979
52. P. Davidson, P. Keller, A. M. Levelut, J. de Phys, 46:939, 1985
53. A. Schoenhals, H. E. Carius, Int. J. Polym. Mater., 45: 239, 2000
54. S. Havriliak, S. Negami, Polymer, 8:161, 1967
55. D. W. Marquardt, J. Soc. Indian Appl. Math., 11:431, 1963
56. L. Toman, P. Vlček, M. Sufčák, A. Pleska, J. Spěváček, P. Holler. Collect Czech Chem Commun; 65:352-60, 2000
57. J. Podešva, J. Spěváček, J. Dybal, J Appl Polym Sci 1999; 74:3214-24.
58. M. Ilavský, R.F.T. Stepto (Eds.), "Polymer Networks: Principles of their Formation, Structure and Properties, 243-87, Thomson Science, London, 1998
59. H. Valentová, Z. Sedláková, M. Ilavský, K. Bouchal, J. Macromol. Sci., Phys; B39:605-22, 2000
60. R. Zentel, G. Strobl, H. Ringsdorf, Macromolecules; 18:960, 1985
61. A. Hofmann et al. Macromolecules, Vol.29, No.1, 129-134, 1996
62. R. Casalini, K. L. Ngai, C. G. Robertson, C. M. Roland, J. Polym. Science: Part B, Vol. 38, 1841-1847, 2000
63. S. Cerveny, R. Bergman, G. A. Schwartz, P. Jacobsson, Macromolecules, 35, 4337-4342, 2002
64. C. A. Angell, J. Res. Natl. Inst. Stand. Technol, 102:171, 1997
65. A. Schoenhals, D. Wolf, Macromolecules, 28:6254, 1995
66. A. Schoenhals, D. Wolf, Polym. Adv. Technol., 7:853, 1997
67. K. L. Ngai, A. Schonhals, J. Polym. Sci. Phys. Ed., 36, 1927, 1998

68. T. M. Roper, C. A. Guymon, E. S. Jönsson, C. E. Hoyle, J. Polym. Sci., A-Polymer Chemistry, 42:6283, 2004
69. D. Demus, J. W. Goodby, G. W. Gray, H. W. Spies, Vill V., (Eds.), “Handbook of Liquid Crystals”, Wiley – VCH, Weinheim, 1998
70. A. S. Govind, N. V. Madhusudana, Eur. Phys. J., E9:107, 2002
71. A. Hofmann, A. Alegria, J. Colmenero, Macromolecules, 29:129, 1996
72. R. Zorn, F. I. Mopsik, G. B. McKenna, L. Willner, D. Richter, J. Chem. Phys., 107:3645, 1997
73. J. F. Mano, J. Macromol. Sci., Part B, 42:1169, 2003
74. M. Mierzwa, G. Floudas, A. Wewerka, Phys. Rev. E, 64, 2001

8. List of Used Variables

σ	stress
$\sigma^*(t)$	oscillatory (complex) stress
σ_0	stress amplitude
γ, ε	strain
η	viscosity
E	Young's modulus
Δ	compression deformation
$\gamma^*(t)$	oscillatory (complex) deformation
γ_0	deformation amplitude
t	time
ω	angular frequency
i	imaginary unit = $\sqrt{-1}$
δ	phase shift
G	modulus
G^*	complex modulus
G'	real (storage) part of complex modulus
G''	imaginary (loss) part of complex modulus
G'_p	superimposed real part of complex modulus
G''_p	superimposed imaginary part of complex modulus
w_E	volume density of elastic energy
w_D	volume density of the dissipative energy
a_{T_0}	horizontal shift factor at reference temperature T_0
τ_T	retardation time at temperature T
T	temperature
T_s, T_0	reference temperatures
T_{VFT}	chosen temperature in VFT equation
T_g	glass transition temperature
T_m	melting temperature
T_{mi}	*i*-melting temperature
ρ	density of polymer
a_{T_s}	horizontal shift factor at reference temperature T_s

C_1, C_2	constants of WLF equation
f_g	fraction free volume at temperature T_g
B	constant of VFT or WLF equation
α_f	coefficient of free volume expansion
f	frequency
ε	permittivity
$\varepsilon'(\omega)$	real part of the complex permittivity
$\varepsilon''(\omega)$	imaginary part of the complex permittivity
$\Delta\varepsilon$	dielectric strength
ε_0	vacuum permittivity ($\varepsilon_0 = 8.85 \cdot 10^{-12}$ F·m^{-1})
ε_γ	relative permittivity
ε_c^*	complex dielectric permittivity
ε_∞	unrelaxed value of the real part of permittivity
M^*	complex electric modulus
M''	imaginary part of the complex electric modulus
M''_{max}	maximum of loss electric modulus in dependence on frequency
M_n	number-average molecular weight
M_w	weight-average molecular weight
p	electric dipole moment
q	charge
r	vector from the negative to the positive charge
μ	permanent induced dipole moment
m_p	induced dipole moment
E_l	intensity of local field
A	polarizability of molecule
P	vector of polarization
κ	susceptibility
D	electric induction
f_{m2}	maxima positions of the loss part of permittivity for the normal relaxation
τ_{star}	normal relaxation time for star-like polymer
τ_{lin}	normal relaxation time for linear chain
a, b	shape parameters of HN equation
f_m	peak frequency (maximum in dependence of loss functions on f)
τ_r	relaxation time
k	Boltzmann constant (=1.38×10^{-23}J/K)

E_a	activation energy
f_∞	pre-exponential frequency factor
f^0	fractional free volume at temperature T_0
$\sigma^*(f)$	complex conductivity
R_0	initial ratio of modification
R_{eGPC}	ratio of modification measured by GPC
R_{eS}	ratio of modification measured by sulfur analyzes
R_{eNMR}	ratio of modification measured by NMR
x_H	amount of hydrogenated-like units
ΔH_m	enthalpy
ΔC_p	changes in the specific heat
α_f	thermal expansion coefficient of the free volume
b_T	vertical shift factor
a_T	horizontal shift factor
$tg\ \delta$	loss tangent
w_S	weight fraction of sulfur